Review Article

Ian Lorenzo E. Gonzaga* and Candy C. Mercado

Copper ternary oxides as photocathodes for solar-driven CO_2 reduction

https://doi.org/10.1515/rams-2022-0043
received March 25, 2022; accepted June 06, 2022

Abstract: The sun's energy, though free and virtually limitless, is a largely unexploited resource, as its conversion into a storable form presents several technological challenges. A promising way of capturing and storing solar energy is in the form of "solar fuels," in a process termed artificial photosynthesis. In a photoelectrochemical (PEC) system, the reduction of CO_2 to carbon-based fuels is driven on the surface of an illuminated semiconductor electrode. Through the decades, many different classes of semiconducting materials have been studied for this purpose, to varying successes. Because of their cheap and abundant nature, semiconducting transition metal oxides are good candidates to realize this technology in an economic scale and have thus attracted considerable research attention. In this review article, the progress achieved with a specific class of metal oxides, namely, the copper ternary oxides such as copper iron oxide and copper bismuth oxide, for PEC CO_2 reduction is examined. Although there have been significant advances in terms of strategies to improve the efficiency and stability of these materials, further studies are warranted to address the many challenges to PEC CO_2 reduction and solar fuel production.

Keywords: artificial photosynthesis, photoelectrochemical CO_2 reduction, semiconductor photoelectrodes, copper oxides, ternary oxides

*** Corresponding author: Ian Lorenzo E. Gonzaga,** Department of Engineering Science, University of the Philippines Los Baños, Los Baños, Philippines; Department of Mining, Metallurgical, and Materials Engineering, University of the Philippines Diliman, Diliman, Philippines, e-mail: iegonzaga@up.edu.ph
Candy C. Mercado: Department of Mining, Metallurgical, and Materials Engineering, University of the Philippines Diliman, Diliman, Philippines

1 Introduction

Solar energy is a free and clean resource abundant enough to supply the world's ever-growing needs [1]. However, due to its diffuse and intermittent nature, it needs to be stored in a transportable form to become a useful energy source [2,3]. In the previous decades, several approaches to harvesting solar power have been developed, to varying levels of technological readiness [3–6]. Among these technologies is the direct storage of the sun's energy in the chemical bonds of a "solar fuel," in a process resembling an artificial photosynthesis system [7–10].

Hydrogen is the simplest solar fuel that can be produced via the splitting of water [11]. However, because hydrogen is a gas at standard conditions, it needs to be compressed and/or liquefied to attain a practical volumetric energy density [12]. Liquid organics that can be produced from the reduction of carbon dioxide (CO_2), such as methanol and ethanol, are easier to handle, more applicable for direct use, and more compatible with the current energy infrastructure [4,5,8,9,12,13]. From this perspective, the solar-driven reduction of CO_2 to fuels as well as other useful chemicals is considered an attractive route for solar energy harvesting and for closing the anthropogenic carbon cycle [12–16].

Before a fully operational system capable of scalable and long-term production of solar fuels is achieved, the thermodynamic and kinetic challenges to the multi-electron reduction of CO_2 need to be addressed [14,17,18]. CO_2, with its two C═O bonds and linear symmetry, is an extremely stable molecule [19–21]. Its endergonic activation requires a significant energy input due to a structural distortion accompanying electron addition [22–24]. Furthermore, the many reaction pathways of the activated CO_2 molecule result in a variety of products, such as formic acid (HCOOH), carbon monoxide (CO), formaldehyde (HCOH), methanol (CH_3OH), and methane (CH_4), making product separation difficult [14–18]. The reduction potentials of CO_2 to these products in aqueous solution, where CO_2 reduction is usually conducted, are given in Table 1. The proximity of the reduction potentials with

Table 1: Reduction potentials at pH 7 of some CO_2 reduction reactions in aqueous solution

Reaction	*E* (vs normal hydrogen electrode (NHE))
$CO_2 + H_2O + 2e^- \rightarrow HCOOH_{(l)} + OH^-$	−0.61
$CO_2 + H_2O + 2e^- \rightarrow CO_{(g)} + 2OH^-$	−0.52
$CO_2 + 3H_2O + 4e^- \rightarrow HCOH_{(l)} + 4OH^-$	−0.48
$CO_2 + 5H_2O + 6e^- \rightarrow CH_3OH_{(l)} + 6OH^-$	−0.38
$CO_2 + 6H_2O + 8e^- \rightarrow CH_{4(g)} + 8OH^-$	−0.25

each other and with the hydrogen evolution reaction (HER) as well as the multiple proton-coupled electron transfers with different kinetic barriers for each step make CO_2 reduction a rather complicated process [25–29].

In a photoelectrochemical (PEC) system, CO_2 reduction is driven on an illuminated semiconductor electrode immersed in a CO_2-saturated electrolyte. The photoelectrode performs the key processes involved in solar fuel generation: absorption of solar energy, charge separation and transport, and catalysis at the surface to make and break chemical bonds [30–35]. As such, there are numerous – and sometimes conflicting – requirements for the photoelectrode: wide range of sunlight absorption, high charge mobility and carrier diffusion length, suitable band energetics, good catalytic activity and selectivity, and long-term stability [33–35]. Many classes of materials, such as the IV, III-V, and II-VI semiconductors, metal oxides, nitrides, oxynitrides, and chalcogenides, and carbon-based materials, have been investigated for PEC CO_2 reduction, yet the desired efficiency, selectivity, and stability are far from being met, even at the laboratory scale [14–16,25–29,33–41]. Developing new photoelectrodes by identifying new materials and designing new architectures therefore remains to be the frontier challenge for PEC CO_2 reduction.

For PEC CO_2 reduction to be realized in a practical scale, the photoelectrode should be made of low-cost, earth-abundant, and non-toxic materials [3,35,42]. Copper-based oxides, generally p-type semiconductors demonstrating a broad absorption of light, are good candidates as photocathodes in this context [43–48]. Because ternary and multinary oxides provide greater flexibility in tuning their properties compared to their binary counterparts, copper ternary oxides have recently gained attention as photocathodes for CO_2 reduction [49–51]. Although research is still lacking, there have already been promising results, making it timely to review the current progress. There have been previous reviews on copper ternary oxides, but none so far has focused on their application for PEC CO_2 reduction [45–51].

This article provides first an overview of the PEC cell and the motivation for the investigation of copper ternary oxides as materials for PEC CO_2 reduction. Then, the latest efforts to improve these materials towards high efficiency and stability photocathodes are examined. Finally, insights on the way forward for these materials, as well as for PEC CO_2 reduction in general, are offered.

2 Photocathode-driven PEC cell

2.1 Overview of PEC cell

The conversion of solar energy to chemical fuel in a solid-state device requires the linking of light absorption and electrochemical functionalities [3,5,6,15,25]. One configuration is a coupled photovoltaic (PV)-electrolysis system, where the PV module performs the light absorption to produce an electric potential that will drive an electrochemical reaction in the electrolyzer. In another configuration, both functionalities are integrated in a single device based on a semiconductor and the solar energy is directly converted into the energy of the redox products. Many authors claim that the latter setup is more favorable from a fabrication and cost standpoint since there will be less stringent material requirements and fewer physical components, although there is a range of intermediate configurations where the device functionalities are partially decoupled [2,5,6,15,27,29,35].

In brief, a semiconductor is a material that possesses a small or modest region (typically between 1–3 eV) of forbidden energy levels called the band gap. When a semiconductor absorbs photons more energetic than its band gap, one of the possible interactions will be for an electron from its valence band to be excited to the conduction band, leaving a hole in the valence band. Following excitation, the photogenerated charges must effectively separate before recombination occurs. This separation can be facilitated by an electric field, such as that formed at the interface of the semiconductor and an electrolyte solution, transports minority charge carriers to the surface and the majority charge carriers to the bulk (or back contact) [52–54]. Accordingly, the role of the semiconductor is primarily to absorb an incident photon, generate an electron-hole pair, and facilitate its separation and transport. Interfacial charge transfer to the adsorbed species to drive the redox reaction is a separate function which may be performed by the semiconductor itself or by a co-catalyst [14–16,55]. A more comprehensive treatment of semiconductor physics and the electrochemical behavior of the semiconductor-electrolyte interface under illumination can be found in refs. [52–54,56,57].

The semiconductor may take the form of micrometer- to nanometer-sized particles suspended in solution (Figure 1a) or a photoelectrode, usually a thin film deposited on a transparent conducting oxide substrate in contact with the electrolyte (Figure 1b) [14,32,34]. In the wireless particulate system (commonly referred to as a "photocatalytic" cell), both reduction and oxidation reactions take place on each particle, but at different sites [14,32,58]. In contrast, the photoelectrode configuration allows for the spatial separation of the reduction and oxidation reactions and for the application of an external bias [33,34]. This system is referred to as a PEC cell (or photoelectrocatalytic/photoelectrosynthetic) as it resembles the two- or three-electrode cell construction for electrochemical systems [14–16,29–35,40,41,53]. It is important to note here that catalysis, by definition, involves a thermodynamically favorable reaction ($\Delta G < 0$), where the catalyst only serves to lower the activation energy (E_A) of the reaction. Thus, the use of the terms "photocatalytic" or "photoelectrocatalytic" in the context of CO_2 reduction, a thermodynamically uphill reaction ($\Delta G > 0$), is imprecise, as pointed out by several authors [5,25,27,59]. In this case, an energy input, which may be provided by incident photons, is used to overcome the thermodynamic barrier ΔG rather than to lower the kinetic overpotential E_A. However, the semiconductor may be considered catalytic in the sense that it can also lower E_A by providing active sites for faster interfacial kinetics. Thus, it is also possible for the reaction to occur at an "underpotential," where the light energy is utilized in such a way that both ΔG and E_A are compensated, resulting in a net negative ΔG of the reaction [60,61].

PEC cell constructions vary depending on the number of photoactive materials and reaction compartments [16,35,38,41,42]. In a single photoelectrode configuration, a photocathode (or photoanode), based on a p-type (n-type) semiconductor, drives the reduction (oxidation) half-reaction, with the other half-reaction taking place on a dark anode (cathode), usually a metal electrocatalyst (such as platinum). The basic operation of a three-electrode PEC cell based on a photocathode is illustrated in

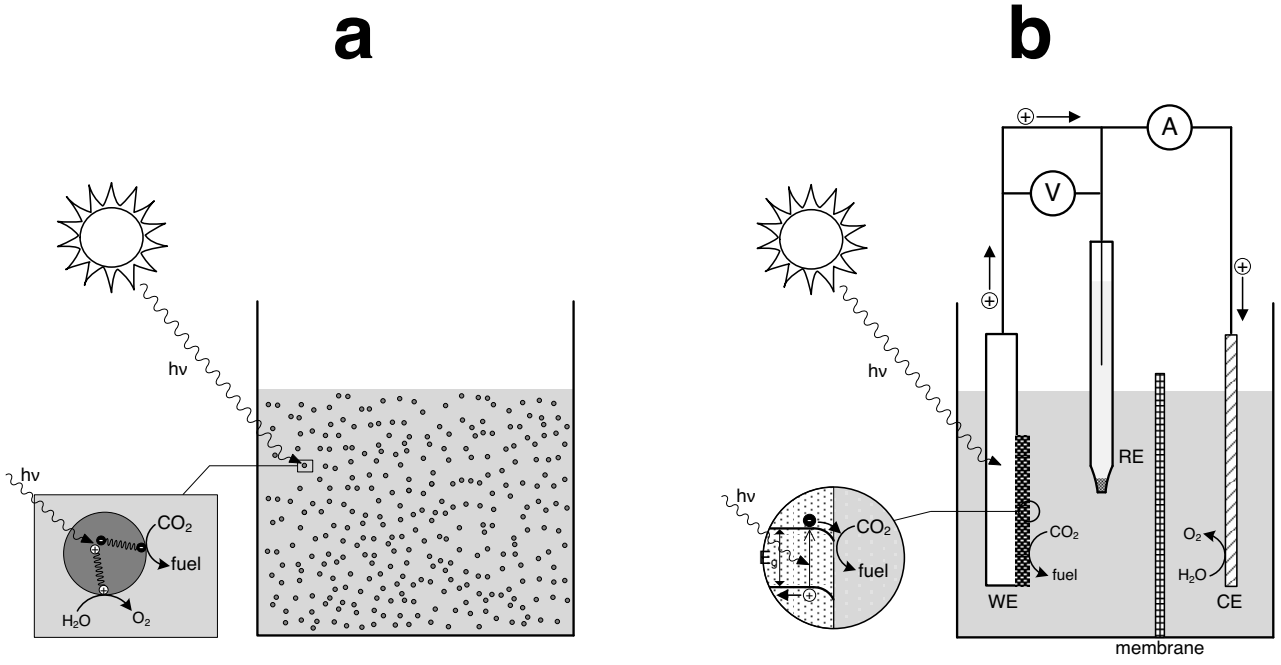

Figure 1: (a) Schematic of a photocatalytic cell, where semiconductor particles are suspended in a CO_2-containing electrolyte. Each particle acts as tiny photoelectrolysis cells where both reduction and oxidation reactions take place. (b) Schematic of a typical two-compartment, three-electrode cell construction of a photocathode-driven PEC cell for CO_2 reduction. Absorption of light (hv) more energetic than the band gap (E_g) of the photocathode results in the generation of electron-hole pairs, separated by the electric field (as shown by the bending of the bands) at the semiconductor-electrolyte interface. Electrons are transported to the surface, where they participate in the reduction of CO_2, while the holes migrate to the back contact and to the counter electrode (CE) via the external circuit, where they are consumed in the oxidation reaction (in aqueous electrolytes, the oxygen evolution reaction), completing the flow of current in the cell. The addition of a reference electrode (RE) allows the potential of the WE (or more specifically, the Fermi level of the photocathode) to be controlled via a potentiostat, which is useful in the investigation of PEC systems. (Adapted with permission from ref. [14]. Copyright © 2015, American Chemical Society).

Figure 1b. A dual photoelectrode configuration is also possible, where the photocathode and photoanode may be in tandem (both semiconductors on a single substrate) or separately illuminated, provided that the semiconductors have matching band gaps and band edge positions [15,35]. Although the ultimate goal for PEC applications is an unbiased cell made of dual photoelectrodes, the photocathode and photoanode can be developed independently [35]. In fact, research on photoanode materials has progressed more and has been the subject of the majority of previous reviews [25,36–39].

2.2 Photocathode materials for CO_2 reduction

PEC CO_2 reduction was first reported by Halmann, who studied a p-GaP photocathode irradiated with UV light in a CO_2-saturated aqueous solution, yielding formic acid (and smaller amounts of formaldehyde and methanol) [62]. Much of the early work on PEC CO_2 reduction involved covalent semiconductors, such as p-GaP [63–66], p-GaAs [63,66–69], p-InP [66,67,70,71], p-CdTe [70,72–74], and p-Si [66,75], being modeled after the several efficient liquid-junction solar cells developed during that period. However, even if their band gaps are suitable for visible light absorption, these semiconductors required extremely negative potentials to effect CO_2 reduction, implying that little to no solar energy was being stored in the products [32]. Modification techniques such as addition of metal co-catalyst [76–79], polymer coating [80,81], and use of solution mediators [82–86] were needed to improve their catalytic activity as well as their stability against corrosion in aqueous electrolyte. These limitations, as well as their high cost and complicated preparation methods, have motivated researchers to explore new classes of materials for PEC CO_2 reduction.

For PEC technology to become economically viable, cheap and earth-abundant materials that can be synthesized using simple and low-cost methods must be used, for which semiconducting transition metal oxides are a good candidate [35,46,49,87,88]. Transition metal oxides are a class of unique materials that exhibit a variety of structures and properties. Depending on the nature of the metal d-orbital, the metal-oxygen bonding can vary between nearly ionic to highly covalent or metallic, resulting in a wide range of electronic behavior, from insulators to semiconductors to superconductors [89,90]. Semiconducting behavior of metal oxides result from intrinsic point defects acting as donor or acceptor states: oxygen vacancies for n-type oxides, while metal vacancies for p-type oxides [90]. Although the first report [91] on the use of semiconducting metal oxides for solar-driven CO_2 reduction came around the same time as Halmann's, research interest had only expanded in the succeeding years, with the advent of nanotechnology and modern computational capabilities [92]. As mentioned earlier, photoanode materials, in particular the most well-studied TiO_2, have received more attention than photocathode materials [25,35–39,49]. This is due in part to the fact that there are fewer p-type oxides because of the localized nature of the oxygen 2p orbitals in the valence band of metal oxides that results in large effective hole masses and easier hole compensation [93]. Even so, the small band gap p-type oxides (and thus suitable as photocathodes), namely, Cu_2O (~2.0 eV) and CuO (~1.5 eV), are susceptible to photocorrosion in aqueous electrolyte [43–48]. Strategies to enhance the stability and PEC activity of Cu_2O and CuO have been demonstrated, such as nanostructuring [94–96], addition of co-catalyst [97–103], deposition of protective overlayers [104–107], and heterojunction formation [61,108–116], to varying successes. The performance of Cu_2O- and CuO-based photocathodes for CO_2 reduction has been reviewed previously [45,46,48] and will no longer be discussed in this article, but a summary of previous findings is presented in Table 2.

Another promising strategy to address the limitations of binary metal oxides is by expanding the search for photoelectrode materials to multinary metal oxides [35,42,46]. The addition of one or more cations to form more complex oxides provides greater flexibility for tuning the optical and electronic properties [42,45]. For ternary and quaternary oxides, more than 8,000 and 700,000 combinations are possible, respectively [49]. With this immense number, it is likely that a semiconductor with the best combination of properties for PEC CO_2 reduction may be found among this group. Like the case with binary oxides, much of the success with ternary oxides has been achieved with photoanodes, specifically $BiVO_4$ [35,46,49,51]. There is still a limited understanding of ternary oxide photocathodes and, even more, their application to PEC CO_2 reduction.

Several copper ternary oxides exhibit p-type behavior, a narrow band gap capable of visible light absorption, and an adequate conduction band potential for CO_2 reduction, as shown in Figure 2. In addition, they appear to be more stable than their binary counterparts, as the additional cation introduces modifications to the electronic structure and to the nature of band transitions that lead to inhibition of Cu self-reduction [49,50]. Along with their inexpensive and nontoxic nature, these copper ternary oxides are good candidates as photocathodes for

Table 2: Cu_2O- and CuO-based photocathodes for PEC CO_2 reduction

Photocathode	Reaction conditions	Products formed	Photostability	Ref.
CuO–Cu_2O nanorods	AM 1.5 illumination (70 mW·cm^{-2}), CO_2-saturated 0.1 M Na_2SO_4	CH_3OH (FE: 95%) at −0.20 V vs standard hydrogen electrode (SHE), 1.5 h	Nanorods remain intact after 2 h photoelectrolysis	[61]
M/CuO/Cu_2O (M = Ag, Au, Cd, Cu, Pb, Sn)	450 W Xe lamp, CO_2-saturated 0.1 M $KHCO_3$	CH_3OH, CO, HCOOH (total FE: 40.45% for M = Pb) at −0.16 V vs SHE, 1 h	70% decrease in photocurrent after 20 min due to reduction of CuO to Cu_2O or Cu	[99]
Cu/Cu_2O	125 W high pressure Hg lamp, CO_2-saturated 0.1 M Na_2CO_3/$NaHCO_3$	CH_3OH, CH_2O, C_2H_5OH, CH_3COH, CH_3COCH_3 (80% total CO_2 reduced) at 0.2 V vs Ag/AgCl, 2 h	—	[100]
Cu_2O/TiO_2/Re(*t*Bu-bipy)$(CO)_3Cl$	450 W Xe arc lamp, CO_2-saturated acetonitrile with 0.1 M $TBAPF_6$	CO (FE: ~100%) at −1.73 V vs Fc/Fc^+, 5.5 h	A small decrease in photocurrent was observed over 5.5 h of testing	[101]
Cu_2O/CuO coated Ag dendrites	Warm white LED (100 mW·cm^{-2}), CO_2-saturated 0.1 M Na_2SO_4	CH_3COO^- (FE: 54%) CO (trace) at −0.4 V vs Ag/AgCl, 1 h	—	[103]
Cu_2O nanowires coated with Cu^+-TiO_2	150 W LS Xe arc lamp, CO_2-saturated 0.3 M $KHCO_3$	CH_3OH (FE: 56.5%), CO, CH_4 (trace) at 0.3 V vs reversible hydrogen electrode (RHE), 2 h	72.4% reduction in the photocurrent after 30 min of testing	[106]
Cu_2O/$Cu_3(BTC)_2$	300 W Xe lamp, CO_2-saturated acetonitrile with 0.1 M $TBAPF_6$	CO (FE: ~95% between −1.77 and −1.97 V vs Fc/Fc^+, STC: 0.83% at −2.07 V vs Fc/Fc^+), 1 h	Nearly constant over 3,500 s at −1.97 V vs Fc/Fc^+	[107]
CuO clusters on Fe_2O_3 nanotubes	Xe lamp (100 mW·cm^{-2}), CO_2-saturated 0.1 M $KHCO_3$	CH_3OH (FE: 91.2%), C_2H_5OH (9.8%), CH_4 (10.46%) at −1.1 V vs SCE, 6 h	—	[108]
Ultra-long CNT/Cu_2O	Solar simulator (100 W), CO_2-saturated 0.1 M Na_2SO_4	CH_3OH (FE: 9%), C_2H_5OH (24%), HCOOH (18%) at 0.05 V vs Ag/AgCl, 4 h	40% reduction in the photocurrent after 4 h of testing	[109]
Ti/TiO_2/CuO	125 W high pressure Hg lamp, CO_2-saturated 0.1 M $NaHCO_3$	CH_3OH (97 mol%), C_2H_5OH, $(CH_3)_2CO$ (trace) at −0.60 V vs Ag/AgCl, 2 h	—	[110]
CuO/g-C_3N_4	Light source (51.6 W·m^{-2}), CO_2-saturated 0.1 M $NaHCO_3$	CH_3OH (FE: 75%, QE: 8.9%) at −0.4 V vs NHE, 4 h	—	[113]
CuO/CdS	250 W lamp, CO_2-saturated 0.1 M $NaHCO_3$	CH_3OH (FE: 86%) at −0.4 V vs NHE	—	[114]
CuO/Cu_2O||rGO|h-WO_3||rGO	150 W solar simulator, CO_2-saturated 0.1 M Na_2SO_4	CH_3OH (FE: ~75%), CO (~25%) at 0.1 V vs RHE, 1 h	rGO layer increased stability of the system, although no actual measurements were shown	[116]

FE – Faradaic efficiency, STC – solar-to-carbon efficiency.

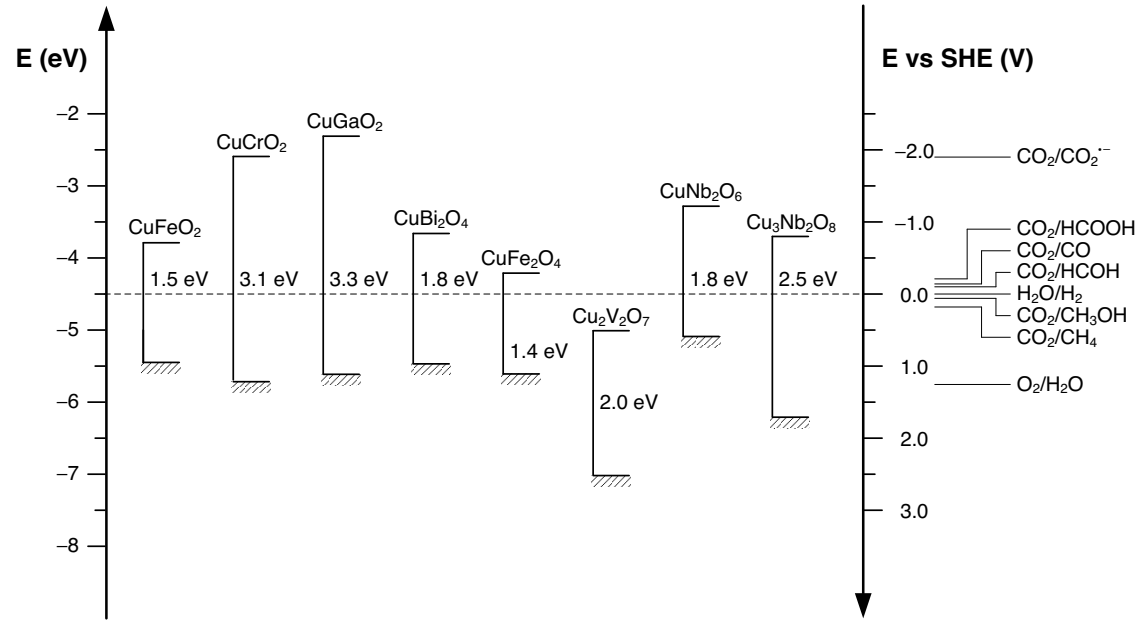

Figure 2: Conduction band and valence band position of several copper ternary oxides relative to CO_2 and water redox potentials, plotted versus vacuum (left) and SHE (right) scales. (Adapted from ref. [50]). Copyright © 2022, IOP Publishing.

CO_2 reduction [51]. Still, several challenges limit the actual performance of copper ternary oxide photocathodes. First is the poor charge separation and transport due to low carrier mobility, a common problem among transition metal oxides [87]. Compared to covalent semiconductors, transition metal oxides are more prone to carrier localization or "self-trapping" due to a strong electron-lattice interaction which causes local lattice distortions called the small polaron. Carrier transport then occurs via a small-polaron hopping mechanism, which is characterized by a very small drift mobility due to its thermally activated nature [117,118]. Next, with the increasing complexity of metal oxides, preparation of stoichiometric, high-quality films becomes more challenging. Even a small percent of sub-stoichiometry can result in large number of defects that can act as recombination centers and diminish the photoactivity [49,51]. Lastly, although there are encouraging results, the long-term stability needed for PEC applications is yet to be demonstrated [50,51].

3 Copper ternary oxide photocathodes

In the following sections, the current progress with copper ternary oxides is summarized and critically examined. In-depth focus is given to the relatively more studied oxides, copper iron oxide ($CuFeO_2$) and copper bismuth oxide ($CuBi_2O_4$), discussing the relation between their crystal and electronic structure, their various preparation methods, the strategies applied to address the aforementioned limitations, and their performance towards PEC CO_2 reduction.

3.1 $CuFeO_2$

$CuFeO_2$ belongs to a group of Cu(I)-based oxides with the delafossite structure and the general formula $CuMO_2$, where M is a metal cation in the trivalent state (M = Al, Co, Cr, Fe, Ga, and Rh) [119]. The delafossite structure comprises of two alternating layers: a planar layer of Cu cations in a triangular pattern and a layer of edge-sharing MO_6 distorted octahedra, where each oxygen is coordinated by one Cu^+ and three M^{3+} cations (Figure 3a and b). Cu and O form linear arrays parallel to the *c*-axis. Depending on the stacking pattern of the MO_6 layers, delafossites form two polytypes, namely, 3R and 2H, that crystallize in the rhombohedral ($R\bar{3}m$) or hexagonal ($P6_3/mmc$) space group, respectively [119,120]. As the band gap of copper delafossites varies widely depending on the M cation, this group of compounds has found a range of electronic applications, including dye-sensitized solar cells, PV and PEC devices, and transparent conducting oxides [45,121].

Among the copper delafossites, $CuFeO_2$ possesses the narrowest optical band gap (1.36–1.55 eV), making it a

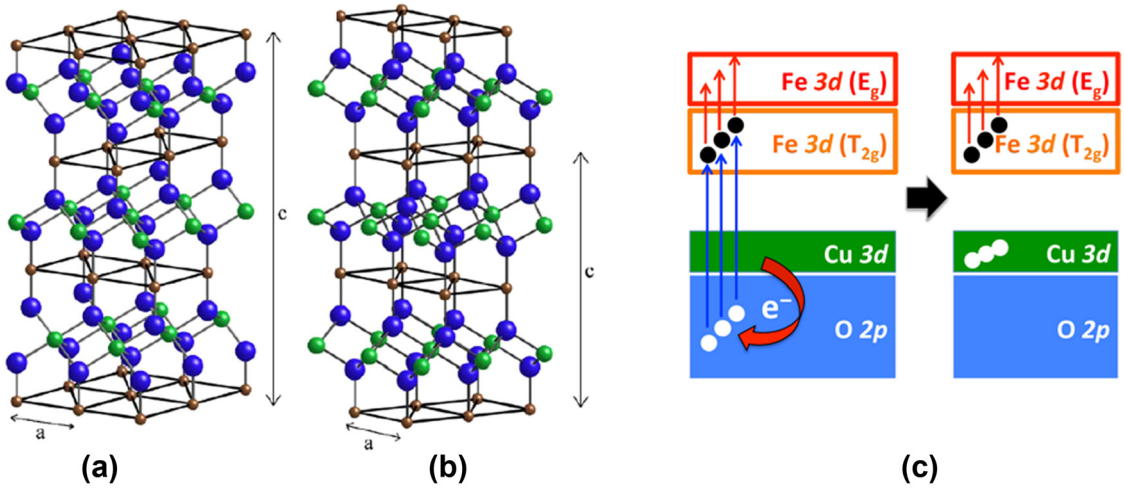

Figure 3: Two polytypes of the delafossite structure: (a) 3R and (b) 2H (brown spheres – Cu, green – M, and blue – O). (Reprinted with permission from ref. [119]. Copyright © 2006, Elsevier). (c) Upon optical excitation of $CuFeO_2$, electrons are promoted from hybridized Cu 3d and O 2p states in the valence band to Fe 3d states in the conduction band. This is followed by an ultrafast hole thermalization where electrons in the higher lying Cu 3d states backfill the photogenerated holes in the lower O 2p states. (Reprinted with permission from ref. [129]. Copyright © 2018, American Chemical Society).

suitable photocathode material for PEC applications [122–124]. It exhibits a p-type conductivity, which is believed to arise from native Cu vacancies and O interstitials in its structure [124–126]. Electronic structure calculations show that the valence band maximum in $CuFeO_2$ is dominated by Cu 3d states, with some degree of hybridization from O 2p states, while the conduction band minimum consists of non-bonding Fe 3d states [127]. The lowest optical transition involves an electron excitation from O 2p states to Fe 3d states [128]. This excitation is followed by an ultrafast thermalization of photogenerated holes from O 2p to Cu 3d valence band states, which may be visualized as an electron transfer from Cu 3d states to backfill holes in the deeper O 2p states [129] (Figure 3c). The hole thermalization process facilitates charge separation in the lattice and suppresses electron-hole recombination (because there is no covalent bonding between the Cu and Fe atoms), and hence, is considered responsible for the greater carrier lifetime, improved stability, and superior photoactivity of $CuFeO_2$ relative to its parent binary oxide, Cu_2O [126,129]. $CuFeO_2$ photocathodes have been prepared using a variety of methods, including hydrothermal synthesis [121,130], electrodeposition [122,126], solid-state synthesis [123,131], sol-gel method [132,133], spray-pyrolysis [134], and reactive co-sputtering [127,135].

Based on its band gap, the theoretically achievable photocurrent of $CuFeO_2$ is 15 $mA{\cdot}cm^{-2}$ (based on AM1.5 illumination), but reported photocurrents are much lower (up to 2.5 $mA{\cdot}cm^{-2}$) [124]. Several studies have been conducted to determine the major limiting factor to the PEC performance of $CuFeO_2$. Time-resolved microwave conductivity measurements found that charge carriers in $CuFeO_2$ are relatively long-lived (as compared to Cu_2O or α-Fe_2O_3), with a time constant of 200 ns [124]. On the contrary, a very short free carrier lifetime (in the order of picoseconds) was measured via time-resolved optical spectroscopy [127]. The results of these two studies indicate that free carriers generated upon illumination quickly self-trap, forming the observed long-lived excited state that is postulated to be electron thermalizing as a surface-trapped small polaron in the Fe 3d conduction band state [136]. As mentioned in the previous section, a conduction mechanism based on small polaron hopping will result in small carrier mobilities. Another factor is the presence of a high density of surface states on $CuFeO_2$, arising from a 10 nm hydroxide or oxyhydroxide surface layer [124]. These surface states act as electron traps, causing severe Fermi level pinning and drastically reducing the photovoltage. Thus, preparation of high-quality films as well as other strategies to address the low carrier mobility and to passivate or remove the surface states is critical to improve the PEC performance of $CuFeO_2$.

To increase its conductivity, $CuFeO_2$ can be doped with a divalent cation (such as Mg^{2+}, Ni^{2+}, and Sn^{2+}), which substitutes with either one Fe^{3+} or three Cu^{+} to contribute additional holes [123,133,137]. Indeed, the hole concentration was found to increase with Mg doping level, but only until a certain threshold where the conductivity of $CuFeO_2$ shifts to n-type, possibly due to charge compensation by oxygen vacancies, an n-type defect [131,133,138].

A 0.05% Mg-doped $CuFeO_2$ was studied for PEC CO_2 reduction, yielding photocurrents of up to 1 mA·cm^{-2} in CO_2-saturated 0.1 M $NaHCO_3$ (pH 6.8) [123]. Formate was observed as the main reduction product (although no quantification was made) in bulk electrolysis experiments performed under blue LED light illumination (470 nm, 2.1 mW·cm^{-2}). However, no comparison in the CO_2 reduction activity between the doped sample and an undoped one was made. Alternatively, carrier concentration can also be increased via oxygen intercalation, which can be achieved via conventional thermal annealing [132] or hybrid microwave annealing [139] of as-synthesized $CuFeO_2$ films. The O interstitials occupy the Cu planes, where there is a large enough space compared to the Fe octahedrons, of the delafossite structure [140]. In one study, the increase in photocurrent of the oxygen-intercalated samples versus as-synthesized $CuFeO_2$ matched that of the acceptor density, which the authors ascribed to an improved charge separation efficiency due to the higher carrier conductivity [132]. On the contrary, another study found that O interstitials have a negative effect on PEC activity of $CuFeO_2$ [126]. Because the O interstitials shift the Cu 3d band to lower energy and the O 2p band to higher energy, the valence band maximum changes from Cu 3d to O 2p upon introduction of the O interstitials, precluding the hole thermalization kinetics responsible for the increased carrier lifetimes in $CuFeO_2$, as discussed above. These conflicting findings suggest the existence of a more complex underlying defect chemistry in $CuFeO_2$ that may require further elucidation. To address the presence of surface traps in $CuFeO_2$ and the slow interfacial kinetics, the addition of a co-catalyst or a protective overlayer has been performed. Noble metals (such as Pt, Ag, and Au) [141,142] and layered double hydroxides [139,143] were employed as co-catalyst, all resulting in an increased photocurrent. Au nanoparticles deposited on diamond-like carbon (DLC) was applied as overlayer for $CuFeO_2$ [142]. In this strategy, the Au nanoparticles contribute to an enhanced light absorption through its surface plasmon resonance whereas the DLC support prevents agglomeration of the Au nanoparticles and decreases charge trapping surface states on $CuFeO_2$. The authors note that further work is needed to optimize the morphology and thickness of the overlayer.

Other approaches to improve the performance of $CuFeO_2$ include formation of novel nanostructures that enhance light absorption and charge separation. $CuFeO_2$-coated amorphous SiO_2 microspheres were assembled on an fluorine-doped tin oxide (FTO) substrate to form a monolayer opal photocathode with glass-like transparency (Figure 4a) [144]. Due to the two-dimensional photonic architecture, the photocathode demonstrated self-light harvesting. Despite the enhanced light absorption, the incident photon-to-current efficiency (IPCE) was low due to the very small thickness (~2 nm) of the $CuFeO_2$ shell that cannot support a depletion layer. To improve the charge separation, the $CuFeO_2$-coated microspheres were coated with an outer shell of $CuAlO_2$, forming a heterojunction between the two oxides [145]. It was initially shown that a host-guest architecture for $CuFeO_2$ and $CuAlO_2$ (a thin film of $CuFeO_2$ on a highly transparent $CuAlO_2$ scaffold) facilitates hole transfer, while blocking electron transfer from the absorber to the scaffold, reducing charge recombination and attaining higher photocurrents [146]. An inverse opal structure was also

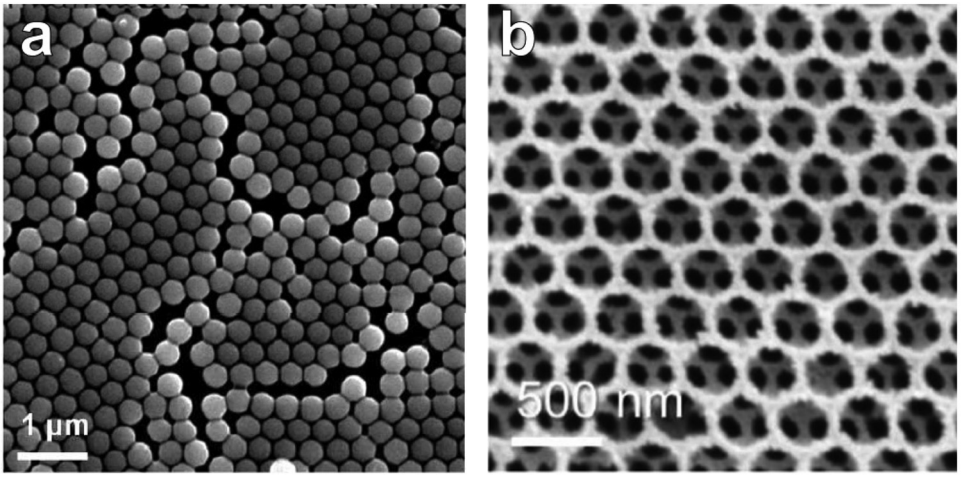

Figure 4: (a) Monolayer of $CuFeO_2$-shelled silica microspheres assembled on FTO. (Reprinted with permission from ref. [144]. Copyright © 2017, American Chemical Society). (b) Top view of inverse opal $CuFeO_2$ on FTO. (Reprinted with permission from ref. [143]. Copyright © 2019, John Wiley and Sons).

constructed for $CuFeO_2$ by the same group of authors (Figure 4b) [143]. In this structure, light absorption was enhanced owing to multiple internal light scattering in the macropores. The inverse opal structure also shortened the electron path to the electrolyte, resulting in a two-fold increase in photocurrent versus that of a planar $CuFeO_2$. In another study, Nb-doped TiO_2 nanotubes were employed as substrate for $CuFeO_2$, creating a p-n composite photocathode for the PEC reduction of CO_2 [147]. Nb doping improved the heat stability of the TiO_2 nanotubes, so that the structure can retain its integrity after the calcination step in the formation of $CuFeO_2$. The authors claimed that a Z-scheme heterojunction was formed, where the weaker photogenerated electrons from TiO_2 recombined with the holes from $CuFeO_2$, allowing the more reductive $CuFeO_2$ electrons to reduce CO_2. Formaldehyde and ethanol were the CO_2 reduction products detected after photoelectrolysis carried out in CO_2-saturated 0.1 M $NaHCO_3$ electrolyte under a 250 W Xe lamp illumination, with ethanol dominating at higher bias potentials.

Several reports have found that composites of $CuFeO_2$ with binary copper oxides (Cu_2O or CuO), typically resulting from nonstoichiometry of precursors during preparation, perform better than phase-pure $CuFeO_2$ [127,148–151]. In particular, $CuFeO_2$/CuO photoelectrodes produced much higher photocurrents than $CuFeO_2$ or CuO alone [127,148]. These studies hypothesize that a type II heterojunction forms between the $CuFeO_2$ and CuO phases. This heterojunction is then responsible for an increased carrier lifetime and presumably, to the observed improved photoactivity of the mixed-phase photoelectrodes. In a proposed scheme (Figure 5), photogenerated electrons from the higher E_{cb} of $CuFeO_2$ can migrate to CuO, whereas those from the lower E_{cb} (an optically forbidden gap) recombine with photogenerated holes from CuO, which cannot effectively perform water oxidation as compared to holes from $CuFeO_2$ [152]. This internal recombination allows for an improved charge separation.

Based upon these findings, an unbiased $CuFeO_2$/CuO-Pt cell under circumneutral pH was devised [148]. The cell produced formate for over a week, with a solar-to-formate efficiency of 0.7–1.2% and Faradaic efficiency of 90%. The $CuFeO_2$/CuO electrode, synthesized via electrodeposition, had a bulk Cu/Fe atomic ratio of 1.4 (measured via inductively coupled plasma-mass spectrometry) and a double-layered structure where $CuFeO_2$ was located in the bottom region, while CuO was uniformly distributed throughout, as determined via transmission electron microscopy-energy-dispersive X-ray spectroscopy. Thus, CuO was segregated as a secondary phase during calcination of the precursor in the presence of air. Notably, the authors did not detect other products (or possibly, were below detection limits), especially H_2 which is known to compete with CO_2 reduction. For comparison, single phase $CuFeO_2$ (Cu/Fe = 1.06) and CuO electrodes were tested under identical experimental conditions. Formate production rates were much lower, and more importantly, O_2 evolution in the Pt counter electrode was observed in neither. In a follow-up study, they investigated the stability of the $CuFeO_2$/CuO photoelectrode for 7 days of PEC testing [150]. X-ray diffraction (XRD) analysis of the used samples showed a decrease in the intensity of $CuFeO_2$ and CuO peaks, while new peaks ascribed to Cu_2O were found, indicating occurrence of cathodic photocorrosion. Reannealing of the used electrodes restores the performance similar to that of the as-synthesized samples. In another study, the effect of varying the Cu/Fe ratio on the selectivity of the CO_2 photoreduction process was investigated [149]. The authors found that decreasing the Cu/Fe

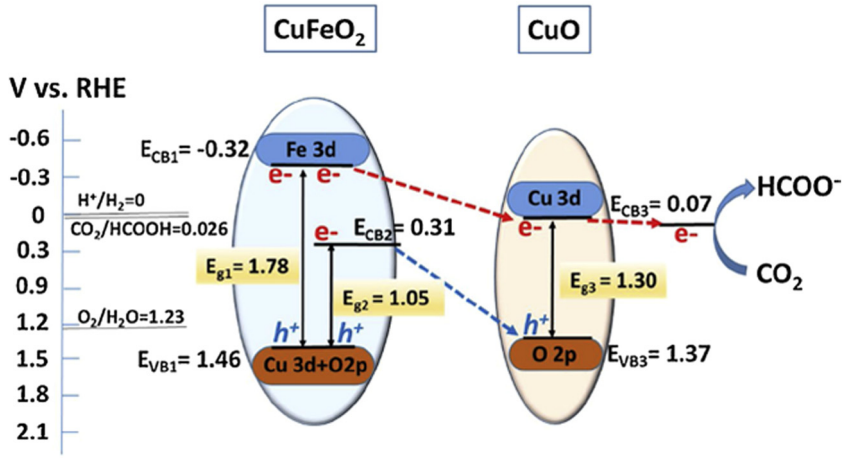

Figure 5: Electronic band diagram of $CuFeO_2$/CuO heterojunction. (Reprinted with permission from ref. [152]. Copyright © 2019, Elsevier).

ratio (more Fe-rich) favors the formation of acetate, a reduction product with C–C coupling. However, a consequence is that the Faradaic efficiency lowers (Figure 6a and b). Because minimal H_2 evolution was observed in all Cu/Fe ratios, the authors attributed the Faradaic efficiency loss to self-reduction of the photocathode. X-ray photoelectron spectroscopy (XPS) of the tested samples revealed almost no surface Fe, even for the most Fe-rich sample. Correspondingly, acetate formation is observed to subside after 10 min of reaction, revealing that surface Fe atoms act as active sites for acetate formation [149].

To provide a theoretical understanding of CO_2 reduction on $CuFeO_2$, the mechanism of CO_2 adsorption and activation on $CuFeO_2$ surface was investigated [153]. In this study, the authors found that the defect-free (011) surface was inert towards CO_2 adsorption but that oxygen vacancies result in a negative charge accumulation on nearby Fe atoms, consequently serving as potential active sites for adsorption. Oxygen vacancies on many metal oxides are well known to play a role in CO_2 adsorption [154]. In another study, the effect of the heterogeneity of the photoelectrode on the selectivity of the PEC CO_2 reduction was investigated [152]. In their DFT calculations, the authors employed two models, a homogeneous structure (HMS) and heterogeneous structure (HTS). The former was based on a homogeneous distribution of Cu, Fe, and O in the entire film (40% $CuFeO_2$ and 60% CuO), while the latter was based on a CuO layer (3 layers) on top of $CuFeO_2$ (2 layers). Bader charge analysis showed that in both the HMS and HTS models, Cu atoms were more enriched with electrons than the surrounding Fe or O atoms, indicating that Cu atoms serve as active sites for the electrophilic CO_2 molecule. Further analysis showed that monodentate coordination of an O atom of CO_2 to a Cu site on the HTS surface was the most kinetically preferred pathway for formate production. Hence, these findings can be correlated to the higher rate of formate production with the heterogeneous $CuFeO_2$/CuO photoelectrodes. Nevertheless, the surface Fe atoms can also act as electron rich sites; however, adsorbed CO_2 on Fe sites are preferentially reduced to surface-bound *CO or *C species that blocks C–H bond formation (a prerequisite to formate production) [155]. This can account for the acetate formation observed in Fe-rich photoelectrodes [149].

3.2 $CuBi_2O_4$

$CuBi_2O_4$ ("kusachiite") is a p-type oxide with a tetragonal crystal structure (space group *P*4/*ncc*). It comprises square planar $[CuO_4]^{6-}$ units stacked along the *c*-axis in a staggered manner, with Bi^{3+} ions positioned between the stacks and connected to six O^{2-} ions with three different bond distances (Figure 7a) [156]. Accordingly, a *c*-axis projection of the crystal structure shows straight channels formed around Bi^{3+} ions (Figure 7b) [157]. The isolated $[CuO_4]^{6-}$ stacks, which are unlike the edge-sharing oxygen octahedra or tetrahedra commonly found in metal oxides, define the unique crystal structure of $CuBi_2O_4$ and play a significant role in its electronic properties [158]. Initially identified as a promising photoactive material in a high-throughput screening study, $CuBi_2O_4$ possesses an optical band gap of 1.5–1.8 eV, making it a good photocathode for PEC devices [157,159].

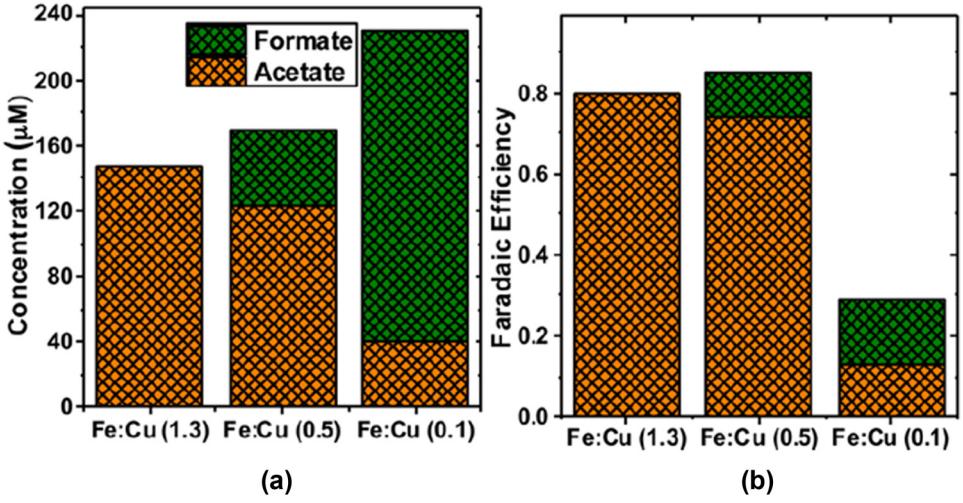

Figure 6: (a) Concentration of formate and acetate and (b) the corresponding Faradaic efficiencies after photoelectrolysis using $CuFeO_2$ electrodes with various Fe:Cu atomic ratios. (Reprinted with permission from ref. [149]. Copyright © 2017, American Chemical Society).

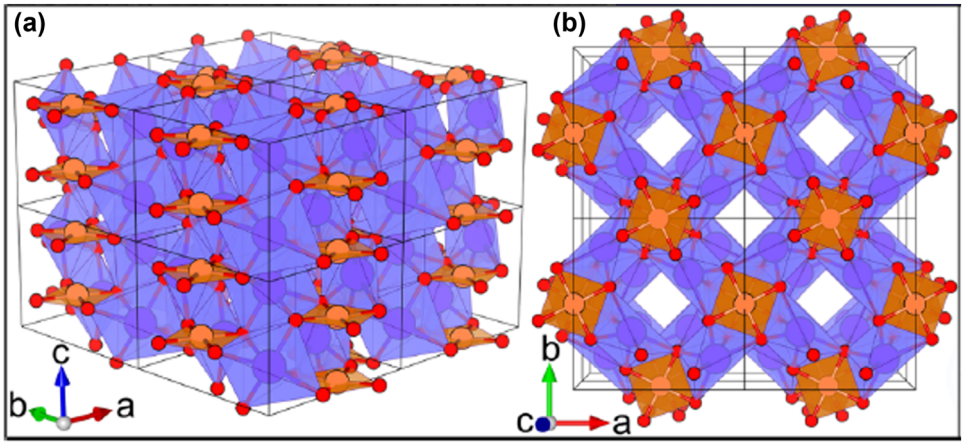

Figure 7: (a) Isometric and (b) *c*-axis projection of the crystal structure of $CuBi_2O_4$ (Cu – orange, Bi – purple, and O – red). (Reprinted with permission from ref. [157]. Copyright © 2021, American Chemical Society).

Unlike in $CuFeO_2$, the Cu ions in $CuBi_2O_4$ adopt a +2 oxidation state and thus, an open shell $3d^9$ configuration that allows intra-atomic electronic transitions [160]. Initially, the valence and conduction band edges of $CuBi_2O_4$ were considered to be primarily of O 2p and Cu 3d character, respectively. Cu vacancies, the most probable defect in $CuBi_2O_4$, introduce states near the valence band edge that gives rise to its p-type behavior [161]. However, a recent first principle and comprehensive spectroscopic characterization study revealed that the valence band maximum and conduction band minimum arise from the occupied and unoccupied spin states, respectively, of the Cu $3d_{x^2-y^2}$ (hybridized with O sp^3 orbitals) that formed from the splitting of Cu 3d levels in the square-planar crystal field of the $[CuO_4]^{6-}$ units [157]. The orbital composition of the valence and conduction bands of $CuBi_2O_4$ is depicted in Figure 8a. Owing to the strong hybridization between Cu 3d and O sp^3 orbitals, Cu 3d character is present across the whole valence band up to the maximum. Contrary to initial reports that the valence band maximum has a significant Bi 6s character, Bi 6s only occurs deep into the valence band. On the other hand, beyond its minimum which consists of the unoccupied Cu $3d_{x^2-y^2}$ spin state, the conduction band is predominantly of Bi 6p character [157,160].

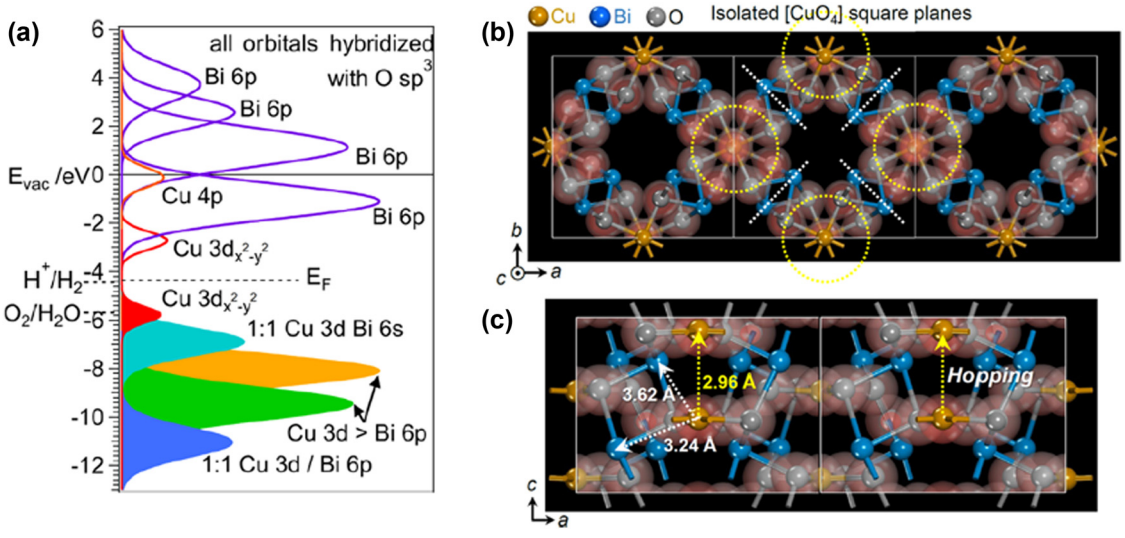

Figure 8: (a) Orbital composition of valence and conduction bands of $CuBi_2O_4$, with the H^+/H_2 and O_2/H_2O redox potentials as reference. (Reprinted with permission from ref. [157]. Copyright © 2021, American Chemical Society). (b) Electron density difference field isosurface contours illustrating lack of overlap of electron density among $[CuO_4]^{6-}$ units. (c) Electron density isosurface in *b*-axis projection, showing Cu–Cu and Cu–Bi interatomic distances and most probable direction of polaron hopping. (b and c reprinted with permission from ref. [158]. Copyright © 2020, American Chemical Society).

Consequently, the lowest-energy optical absorption in $CuBi_2O_4$ corresponds to a Cu d–d excitation, not the O 2p to Cu 3d charge transfer transition initially proposed [161]. While the Cu d–d transition accounts for the low-energy visible light absorption of $CuBi_2O_4$, it does not significantly contribute to the photoresponse, as localized d–d transitions are known to be less efficient in converting photons to photocurrent than O^{2-} ligand to metal cation charge transfer (LMCT) transitions in open-shell metal oxides [157]. This can very well explain why even though $CuBi_2O_4$ exhibits an absorption onset at low energies (1.5–1.8 eV), the IPCE and absorbed photon-to-current efficiency become practically significant only at higher energies (1.8–2.25 eV), as reported in many experimental studies [156,162–168]. Meaningful photocurrent generation in $CuBi_2O_4$ requires the absorption of higher energy photons that brings about the O 2p to Cu 3d LMCT transition (or O 2p to Bi 6p at even higher energies) [160].

Due to the nature of the optical transitions, the photogenerated electrons and holes are confined in the $[CuO_4]^{6-}$ units that are isolated from each other, as mentioned above (Figure 8b). Consequently, there is a lack of DOS overlap among $[CuO_4]^{6-}$ units that would serve as conduction paths for the minority and majority carriers. This results in a localization of electrons at discrete Cu sites, and hence, to polaron formation that is stabilized in part because of the attainment of a transient stable electronic configuration (from Cu^{2+} $3d^9$ to Cu^{+} $3d^{10}$). Consequently, electronic conduction in $CuBi_2O_4$ proceeds via small-polaron hopping between $[CuO_4]^{6-}$ units along the *c*-axis, as the nearest cation to Cu is another Cu along the *c*-axis (Figure 8c) [156,158]. Similar to previous discussions, this small-polaron hopping conduction mechanism is responsible for the poor charge carrier transport in $CuBi_2O_4$. Based on its band gap of 1.5–1.8 eV, the maximum theoretical photocurrent for $CuBi_2O_4$ under AM1.5 illumination is 19.7–29.0 $mA{\cdot}cm^{-2}$ [164]. Actual photocurrents are therefore expected to be lowered by the inferior charge transport, and even more by the sluggish CO_2 reduction interfacial kinetics [157]. Therefore, strategies to address the inherent limitations of $CuBi_2O_4$ are requisite for $CuBi_2O_4$ to be a suitable photocathode for PEC applications.

To achieve superior PEC performance, preparation of high quality $CuBi_2O_4$ photocathodes is of foremost importance. $CuBi_2O_4$ films have been prepared using simple techniques such as electrodeposition [162,166,169], drop-casting [156,170,171], and spin-coating [167,168]. However, these techniques usually resulted in incomplete surface coverage, which can reduce the photoactivity because exposed FTO can act as sites for back reactions [172,173]. In addition, nanoscale phase impurities that are potentially deleterious to the integrity of the photoelectrode and that may not be detected by XRD can also be formed [174]. More advanced techniques such as spray pyrolysis [173], reactive co-sputtering [157,175], and pulsed laser deposition [176,177] yielded highly phase-pure, homogeneous $CuBi_2O_4$ films. Furthermore, phase-purity was better achieved with rapid thermal processing (RTP) (10 min at 650°C) than conventional furnace heating (CFH) (72 h at 500°C) of pulsed-laser-deposition-prepared CuO/Bi_2O_3 precursor [178]. This finding was attributed to nucleation and grain growth processes during heating (Figure 9a). The high heating rate in RTP rapidly brings the CuO/Bi_2O_3 precursor to a high-temperature steady state that enables fast diffusion of Cu ions into the Bi_2O_3 layer. This yields a homogeneous distribution of $CuBi_2O_4$ nucleation sites after 5 min; rapid grain growth then results in the formation of a single-phase $CuBi_2O_4$. In contrast, the slower heating rate in CFH causes grain growth to occur even while Cu diffusion is still taking place. The resulting $CuBi_2O_4$ grains impede further diffusion so that phase transformation of the precursor is incomplete.

Carrier diffusion length in $CuBi_2O_4$ was found to be in the order of 10–60 nm, as determined from time-resolved microwave conductivity measurements [156]. Compared to the light penetration depth of 244 nm (for a wavelength of 550 nm), the short carrier diffusion length leads to excessive electron-hole recombination, severely limiting the PEC performance [156,164]. As with other photoelectrodes, the diffusion pathway of charge carriers can be shortened through nanostructuring, which may also increase internal light scattering and active sites for interfacial reactions [34–40]. Recently, a novel template-assisted synthesis strategy was devised to prepare a $CuBi_2O_4$ film with a nanodendritic structure, with the trunks and subbranches having a radius around 90–150 nm (Figure 9b) [179]. The nanodendritic $CuBi_2O_4$ demonstrated a photocurrent (measured in N_2-saturated 0.1 M Na_2SO_4 electrolyte under AM1.5 G illumination) twice that of a planar film, which the authors ascribed to a shorter diffusion length of the $CuBi_2O_4$/electrolyte interface as well as a higher specific surface area. To improve its photostability, the nanodendritic $CuBi_2O_4$ was conformally coated with a TiO_2 protective overlayer.

Enhancing hole transport to minimize electron-hole recombination can significantly improve the performance of $CuBi_2O_4$ photocathodes. To this end, doping and use of hole transport layers have been investigated. Doping of $CuBi_2O_4$ with Ag resulted in an increase in hole concentration, as substitution of Ag^{+} with Bi^{3+} is charge-compensated by free holes (no Ag impurities were formed) [172].

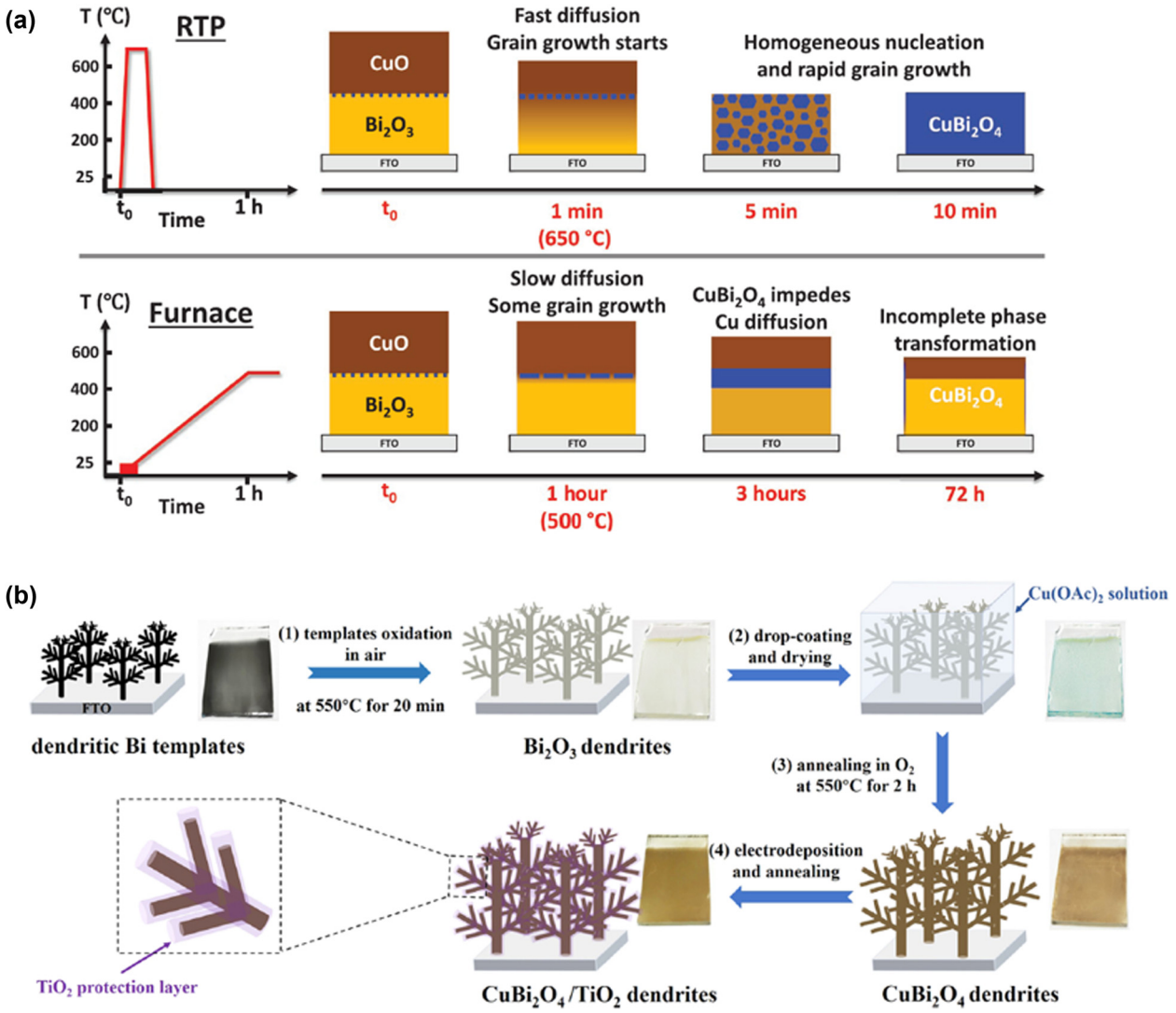

Figure 9: (a) Comparison of the diffusion, nucleation, and grain growth processes during the formation of $CuBi_2O_4$ via rapid thermal processing and conventional furnace heating. (Reprinted from ref. [178]). (b) Scheme of preparation of nanodendritic $CuBi_2O_4$ (with TiO_2 as protection layer). (Reprinted with permission from ref. [179]. Copyright © 2021, American Chemical Society).

Owing to the enhanced hole transport, Ag-doped $CuBi_2O_4$ exhibited higher photocurrent and better stability (against anodic photocorrosion) than undoped $CuBi_2O_4$ [172]. Hole transport layers (HTL) address the mismatch between the work function of FTO (a degenerately doped n-type semiconductor), the most commonly employed conducting substrate, and the Fermi level of the semiconductor photoelectrode. Due to such mismatch, a Schottky barrier may form at the FTO/$CuBi_2O_4$ interface, impeding hole collection in the back contact and enhancing carrier recombination [180]. Gold [162] and Cu-doped NiO [180] were found to be effective HTLs for $CuBi_2O_4$. The energy band alignment of the FTO/Cu:NiO/$CuBi_2O_4$ photocathode is shown in Figure 10a.

Another strategy to improve the PEC cell performance of $CuBi_2O_4$ is the addition of conformal protective overlayers to address its photocorrosion. The function of the overlayer should not be limited to passivation of surface states and blocking of $CuBi_2O_4$/electrolyte contact; ideally, the overlayer should also act as an electron-selective contact that enhances charge separation [181,182]. Like in HTLs, addition of an overlayer will require a precise engineering of the interface such that energy levels are properly aligned and that no recombination traps are formed [175]. To this end, the multilayer scheme initially developed for Cu_2O [104] was adopted for $CuBi_2O_4$ with CdS as the buffer layer between $CuBi_2O_4$ and the TiO_2 protection layer [181]. In another study, high throughput

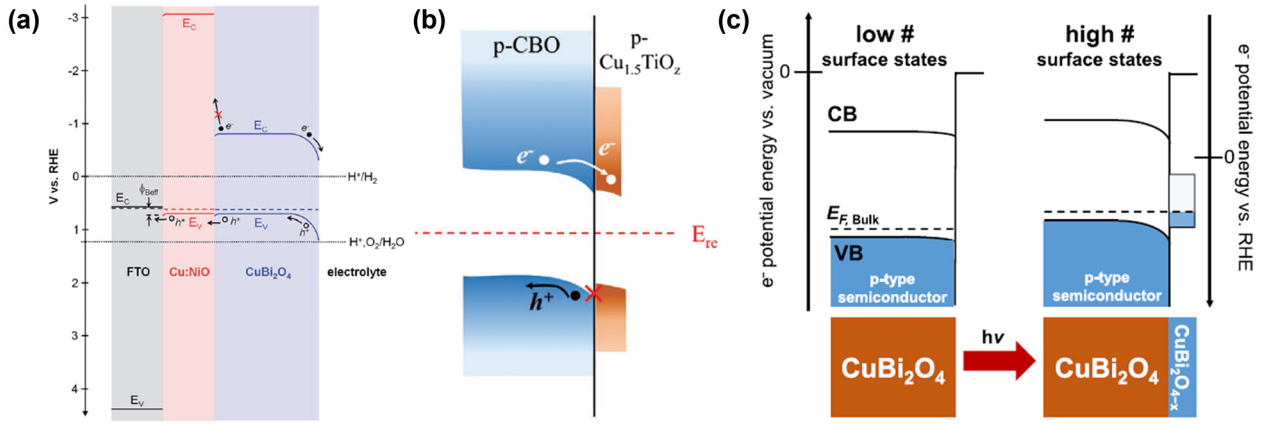

Figure 10: (a) The favorable alignment of the energy levels of FTO/Cu:NiO/$CuBi_2O_4$ facilitates hole transport to FTO, while blocking electrons from reaching FTO. (Reprinted from ref. [180]). (b) Band alignment of $CuBi_2O_4$/$Cu_{1.5}TiO_z$ interface, showing favorable electron transport to the overlayer. (Reprinted with permission from ref. [175]. Copyright © 2020, John Wiley and Sons). (c) Introduction of surface states on $CuBi_2O_4$ upon irradiation resulted in a shift in Fermi level and an increased band bending. (Reprinted from ref. [182]).

methodology was employed to identify a suitable multinary metal oxide overlayer for $CuBi_2O_4$ [175]. An optimized $Cu_{1.5}TiO_z$ overlayer was well-matched with $CuBi_2O_4$, forming a heterojunction that favored electron transport to the surface (Figure 10b). A unique, facile approach to introduce a protective overlayer on $CuBi_2O_4$ involves its pre-irradiation to form reduced Cu states on its surface [182]. The surface states induce an additional downward band bending upon illumination that contributes to improved charge transport and hence PEC cell performance (Figure 10c).

Tailoring the Cu/Bi ratio to deliberately introduce phase impurities has also been applied as a strategy to achieve better PEC cell performance of $CuBi_2O_4$. Similar to $CuFeO_2$, nonstoichiometric $CuBi_2O_4$ films likely contain binary oxide phases, that is, CuO if Cu/Bi >1/2 or α,β-Bi_2O_3 otherwise, since $CuBi_2O_4$ is a line compound (there is no $Cu_xBi_{2-x}O_4$ solid solution) [174]. Because CuO and Bi_2O_3 are both photoelectrochemically active, the electronic and optical properties of these nonstoichiometric films can be tuned with the Cu/Bi ratio [163]. Since CuO has a narrower band gap (~1.5 eV), the optical band gap redshifts and the films become progressively darker with higher Cu/Bi ratio [183]. Also, with higher Cu/Bi ratio, the flat band potential shifts to less positive values (away from valence band) because of a lower Cu vacancy concentration (recall that Cu vacancies introduce p-type behavior of $CuBi_2O_4$) [164,167,175]. Taking advantage of this concept, a photocathode with a Cu/Bi ratio gradient across its thickness was devised by placing into contact three films of varying stoichiometries (Cu/Bi = 1/3, 1/2, and 1) and thus, varying Fermi levels (Figure 11a) [164]. When placed in contact, the Fermi levels of the three films equilibrate by distributing the free holes, so that the conduction and valence bands bend at each interface (Figure 11b). The forward-gradient film, that is, with Cu/Bi ratio increasing from substrate side to electrolyte side (or Cu vacancy concentration decreasing), exhibited the correct band bending where photogenerated holes are transported to the FTO back contact, while the electrons are transported to the surface (Figure 11c), and resulted in the best photoresponse versus a homogeneous and a reverse-gradient film.

Indeed, composites of $CuBi_2O_4$ with its secondary oxide CuO, both as randomly intermixed [163,168] or as separate layers [184,185], have demonstrated better PEC cell performance than $CuBi_2O_4$ or CuO alone. The simultaneous formation of both $CuBi_2O_4$ and CuO phases from a common precursor ensures a sufficient interfacial contact between the two phases, a requirement to establish an effective heterojunction [163,185]. However, the exact alignment of the heterojunction is still unclear. In one study, a layered CuO/$CuBi_2O_4$ was synthesized where $CuBi_2O_4$ acts as the electrocatalytic phase and as a protective layer for the relatively less stable CuO [184]. The authors claimed that a type II heterojunction forms at the interface, where photogenerated electrons are injected to $CuBi_2O_4$, while the holes to CuO (Figure 12a). In a different study, a $CuBi_2O_4$/CuO heterojunction with CuO deposited on $CuBi_2O_4$ was prepared [185]. CuO and $CuBi_2O_4$ still exhibited a type II alignment but with electron flow towards CuO (Figure 12b). Aside from CuO, composites of $CuBi_2O_4$ with Bi_2O_3 [163,186,187], as well as other oxides [188,189], have been reported in literature with varying successes in the improvement of PEC activity.

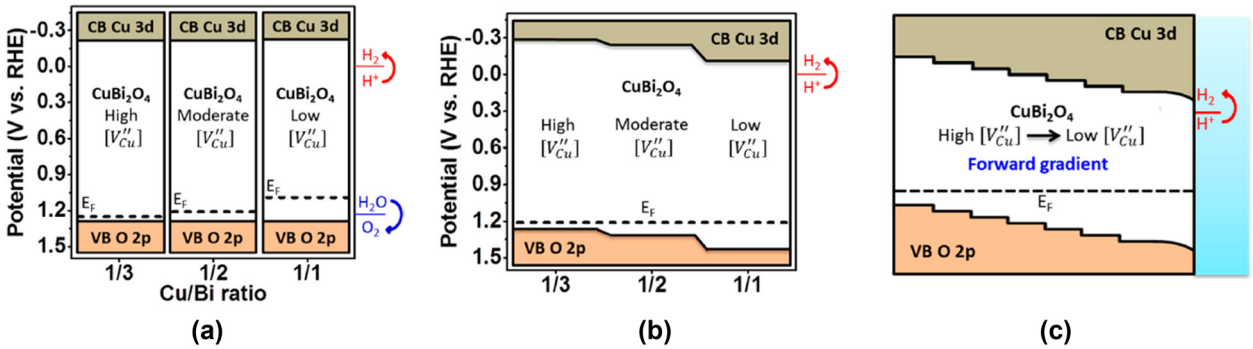

Figure 11: (a) Band positions of nonstoichiometric $CuBi_2O_4$ films before contact. (b) Equilibration of Fermi levels and corresponding band bending at the interfaces upon contact. (c) Formation of $CuBi_2O_4$ with forward gradient. (Reprinted with permission from ref. [164]. Copyright © 2017, American Chemical Society).

Despite this significant progress with $CuBi_2O_4$, majority of the efforts were directed towards H_2O reduction; studies on the improvement of $CuBi_2O_4$ as a photocathode for CO_2 reduction are few. Electrodeposited $CuBi_2O_4$ films were studied for the PEC reduction of CO_2 [166]. The film thickness was first optimized based on the tradeoff between an enhanced light absorption and an increase in number of recombination centers. The optimized sample was used as photocathode for CO_2 reduction (in a CO_2-saturated 0.1 M $KHCO_3$ electrolyte, under a 300 W Xe lamp illumination and a bias of 0 V vs Ag/AgCl). CO was the only detected product in the headspace after 4 h of reaction, but with a very low yield (0.0155 μmol·cm^{-2}). In another study, no product was even detected despite the conduction band being in a thermodynamically feasible position for CO_2 reduction [190]. These results indicate that aside from the inherently poor charge transport kinetics, the bare $CuBi_2O_4$ surface shows little activity for CO_2 reduction and that similar strategies to those discussed in the preceding paragraphs are necessary to drive CO_2 reduction on $CuBi_2O_4$.

TiO_2 was employed as a protective overlayer on nanoporous $CuBi_2O_4$, using two different overlayer thicknesses (50 nm and 1 μm) [191]. However, TiO_2 was not conformally deposited on the $CuBi_2O_4$ surface; there were regions where there was contact between $CuBi_2O_4$ and the electrolyte. CO and H_2 were the detected products in PEC measurements in a CO_2-saturated bicarbonate electrolyte under an applied bias of −0.50 V (vs reversible hydrogen electrode (RHE)). Measured photocurrents and the overall yield were both larger for the sample with thicker TiO_2 due to a more efficient charge separation versus the sample with thinner TiO_2, where the space-charge region in the TiO_2/electrolyte interface cannot be fully supported by the thin overlayer. However, selectivity for CO was lower for the sample with thicker TiO_2 layer; the authors attributed this to the effect of the nanostructure on mass transport (Figure 13). In the

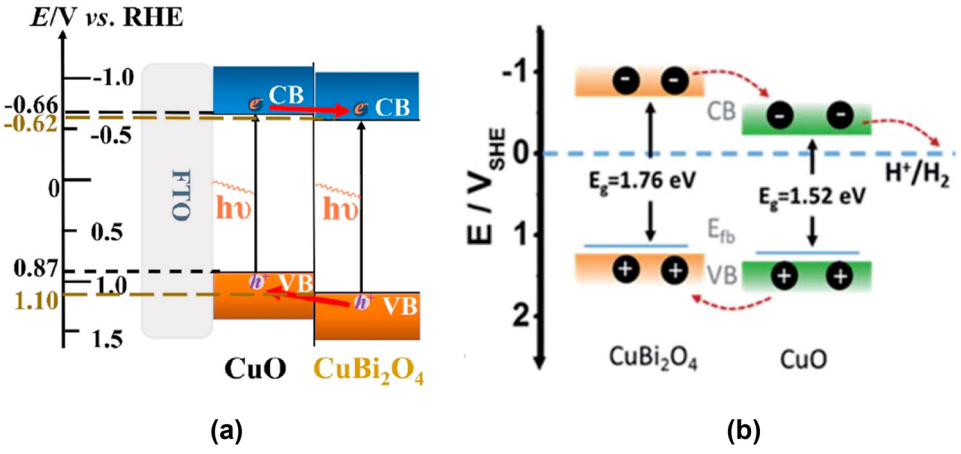

Figure 12: Proposed energy band alignments of the $CuBi_2O_4$/CuO heterojunction: (a) electron moves from CuO to $CuBi_2O_4$ to electrolyte (Reprinted with permission from ref. [184]. Copyright © 2021, Elsevier) and (b) electron moves from $CuBi_2O_4$ to CuO to electrolyte (Reprinted from ref. [185]. Copyright © 2020, Royal Society of Chemistry).

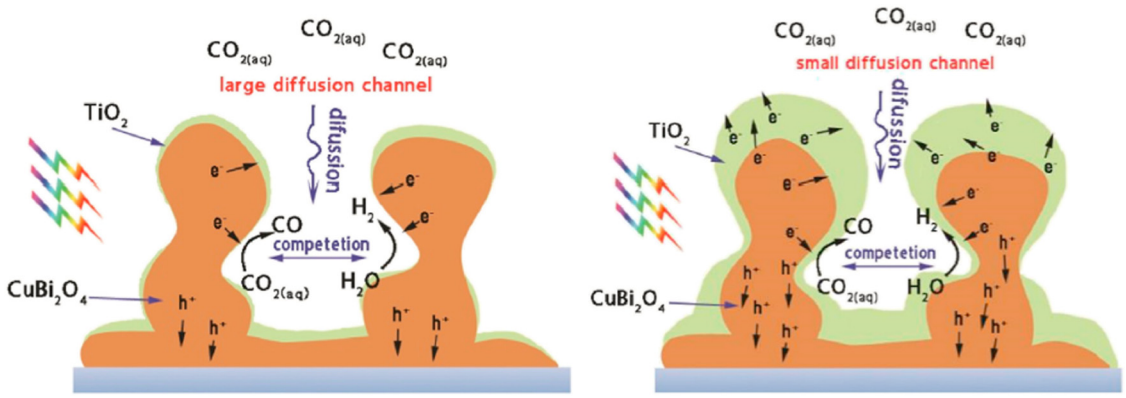

Figure 13: Effect of mesostructure on activity and selectivity of $CuBi_2O_4/TiO_2$ nanocomposite for PEC reduction of CO_2. (Reprinted with permission from ref. [191]. Copyright © 2021, Elsevier).

sample with thicker TiO_2 layer, the channels or pores were narrower so that local pH changes near the interface were more pronounced. Because CO_2 reduction is more favored at higher pH, CO_2 is more quickly exhausted near the interface, and the process becomes mass transfer limited. Consequently, the electrons are instead consumed for the HER.

3.3 Other copper ternary oxides

Other copper delafossites, namely, $CuCrO_2$ and $CuGaO_2$, have been investigated as photocathodes for CO_2 reduction. $CuCrO_2$ is, however, a wide band gap p-type semiconductor (2.95–3.15 eV) implying that UV illumination is necessary to obtain a photoresponse [192]. $CuCrO_2$ prepared via solution combustion synthesis was tested for its photoactivity towards CO_2 reduction [193]. The as-synthesized sample contained phase impurities, namely, CuO (4 wt%) and α-Cr_2O_3 (6 wt%); annealing in Ar at 700°C allowed the formation of a more phase-pure sample. As expected, onset of IPCE was near the UV region (438 nm). Long-term photoelectrolysis of the Ar-annealed sample in CO_2-saturated bicarbonate, under UV illumination, resulted in the formation of CO, CH_4, and H_2 in the gas phase, while HCOOH and CH_3OH in the liquid phase, with a total Faradaic efficiency of 85–90%. Although photocurrents decreased significantly after one hour, the authors claimed that their $CuCrO_2$ photocathode was relatively more stable than Cu_2O. Because unmodified $CuCrO_2$ was proven capable of CO_2 reduction, there is much room for improvement especially by making it responsive to visible light. $CuGaO_2$ is another wide band gap p-type semiconductor (3.3–3.75 eV) which has been employed as hole transport layer in dye-sensitized solar cells [194,195]. The photochemical activity (in powder form) of $CuGaO_2$ and its solid solution with $CuFeO_2$ and $CuGa_{1-x}Fe_xO_2$ towards CO_2 reduction was investigated [194]. The indirect band gap of 2.55 eV in pure $CuGaO_2$ (which was not previously observed in thin film $CuGaO_2$) was observed to shift to 1.5 eV upon Fe alloying, due to a crystal strain that modifies the electronic structure of $CuGaO_2$. Observed reduction products from an aqueous CO_2 solution upon illumination with broadband light were CO and CH_4 (trace). However, the amount of CO evolved did not correlate with the degree of Fe substitution, so it is likely that the indirect band gap absorption does not result in an efficient charge separation and accordingly contribute to the photocatalytic process. In a different study, $CuGaO_2$ was employed as a scaffold for a Ru(II)–Re(I) supramolecular photocatalyst for CO_2 reduction [196]. PEC testing using the hybrid photocathode in a CO_2-saturated aqueous solution under visible light irradiation (>460 nm) produced both CO and H_2, with a total Faradaic efficiency of 81%. A PEC cell employing the Ru(II)–Re(I)/$CuGaO_2$ hybrid photocathode coupled to a CoO_x/TaON photoanode with a Z-scheme configuration was then devised. Under visible light illumination and bias-free condition, CO and H_2 were produced at the cathode, while O_2 evolution was observed at the anode.

Other Cu^{2+}-based ternary oxides that have been investigated as photocathodes for CO_2 reduction are $CuFe_2O_4$, $Cu_2V_2O_7$, and the copper niobates $CuNb_2O_6$ and $Cu_3Nb_2O_8$. $CuFe_2O_4$ is a ternary oxide with an inverse spinel structure and a band gap of 1.39–1.42 eV. Methanol was the only product detected in the liquid phase from PEC reduction in a CO_2-saturated bicarbonate solution under visible light irradiation (>470 nm), with a corresponding Faradaic efficiency of 62% [197]. Addition of CdS [198], graphene oxide [199], and polyaniline (PANI) [200] as co-catalysts resulted in a better PEC performance, as reflected in the higher IPCEs of 12.09, 8.02, and 7.1% (at 470 nm), respectively,

Table 3: Ternary copper oxide photocathodes for PEC CO_2 reduction

Photocathode	Reaction conditions	Products formed	Photostability	Ref.
(a) $CuFeO_2$				
Mg-doped $CuFeO_2$	Blue LED illumination (470 nm, 2.1 mW·cm^{-2}), CO_2-saturated 0.1 M $NaHCO_3$	$HCOO^-$ (FE: 10%) at −0.9 V vs SCE, 8–24 h	—	[123]
$CuFeO_2$/CuO	150 W Xe arc lamp, CO_2-saturated 0.1 M $KHCO_3$	$HCOO^-$ (~1% solar-to-formate efficiency, 90% selectivity) using a two-electrode system (no external bias)	Formate production continued over 17 days, but rate is reduced by 60%; reannealing of the photoelectrode restored its activity	[148,150]
$CuFeO_2$/CuO	Warm white light LED (100 mW·cm^{-2}), CO_2-saturated 0.1 M $KHCO_3$	CH_3COO^- (FE: 80%) at −0.4 V vs Ag/AgCl, 2 h	Acetate formation quickly deactivates after first 10 min of testing due to dissolution of Fe	[149]
$CuFeO_2$/Cu_2O nanorods	300 W Xe arc lamp, CO_2-saturated 0.5 M $KHCO_3$	CH_3COO^- (FE: 68.6%), $HCOO^-$(21.6%) at 0.35 V vs RHE, 30 min	Photocurrent decreased by 8% after 10 LSV repetitions	[151]
$CuFeO_2$/Nb-doped TiO_2 nanotubes	250 W Xe arc lamp, CO_2-saturated 0.1 M $NaHCO_3$	C_2H_5OH, CH_2O at −0.4 V vs SCE, 5 h	—	[147]
(b) $CuBi_2O_4$				
$CuBi_2O_4$	300 W Xe lamp, CO_2-saturated 0.1 M $KHCO_3$	CO (0.0155 μmol·cm^{-2}) at 0 V vs Ag/AgCl, 4 h	—	[166]
Au-decorated $CuBi_2O_4$	300 W Xe lamp, CO_2-saturated 0.1 M $KHCO_3$	No product detected	—	[190]
$CuBi_2O_4$/TiO_2	300 W Xe lamp, CO_2-saturated 0.1 M $KHCO_3$	CO at −0.5 V vs RHE	—	[191]
(c) Other Cu ternary oxides				
$CuCrO_2$	300 W Hg-Xe arc lamp, CO_2-saturated 0.1 M $NaHCO_3$	CO (5.9%), HCOOH (2.7%), CH_3OH (0.5%), CH_4 (0.7%) at 0 V vs RHE, 4 h	Photocurrent decreased substantially after 1 h of testing	[193]
$CuGaO_2$/Ru(II)-Re(I)	300 W Xe lamp, CO_2-saturated 0.05 M $NaHCO_3$	CO (FE: 72% for total cathodic reaction including H_2 evolution) in a non-biased cell with CoO_x/TaON as photoanode	About 80% of the Ru(II)-Re(I) catalyst lost electrochemical activity after 15 h	[196]
$CuFe_2O_4$	XD 300 high brightness cold light, CO_2-saturated 0.1 M $NaHCO_3$	CH_3OH (FE: 87% for $CuFe_2O_4$/GO at −0.4 V vs Ag/AgCl, 72% for $CuFe_2O_4$/CdS at −0.35 V vs Ag/AgCl, 73% for $CuFe_2O_4$/PANI at −0.4 V vs Ag/AgCl)	For $CuFe_2O_4$/GO, little decrease in CO_2 reduction yield after 4 cycles of testing	[198–200]
$Cu_3Nb_2O_8$	Solar simulator (100 mW·cm^{-2}), CO_2-saturated 0.5 M $NaHCO_3$	CO (FE: 9%) at −0.2 V vs Ag/AgCl, 20 min	Rapid decrease in photocurrent after 800 s due to reduction of Cu; reannealing restores initial photocurrent	[203]

FE, Faradaic efficiency.

Table 4: Copper chalcogenide photocathodes for PEC CO_2 reduction

Photocathode	Reaction conditions	Products formed	Photostability	Ref
$CuInS_2$/graphene	Xe lamp (100 mW·cm^{-2}), 0.1 M acetate buffer	CH_3OH (95%) at −0.59 V vs SCE, 5 h	No change in morphology and structure was detected after 10 h testing	[215]
$CuInS_2$/CuO/CuS	Xe lamp (100 mW·cm^{-2}), 0.1 M acetate buffer with 10 mM pyridine	CH_3OH (86.8%) at −0.60 V vs SCE, 1.5 h	No significant change in the crystalline structure after 4.5 h testing, but particle size became smaller	[216]
$CuInS_2$/Cu-In	Xe lamp (100 mW·cm^{-2}), 0.1 M $KHCO_3$	C_2H_5OH (FE: ~90%), CH_3OH (trace) at −0.70 V vs SCE, 1.5 h	—	[217]
$CuInS_2$/$CuFeO_2$	Xe lamp (100 mW·cm^{-2}), 0.1 M acetate buffer with 10 mM pyridine	CH_3OH (88%) at −0.70 V vs SCE, 1.5 h	Rate of methanol formation remains almost constant within 9 h and then decreases	[218]
$CuGaS_2$/CdS/TiO_2	150 W solar simulator lamp, 0.1 M Na_2SO_4	CH_3OH (65 mol%), C_2H_5OH (22.5%), $(CH_3)_2CO$ (12.5%) at −0.70 V vs Ag/AgCl, 4 h	CH_3OH, C_2H_5OH, and $(CH_3)_2CO$ productions dropped by 12%, 56%, and 60% in 2nd use of photocathode	[219]
$CuGa_3Se_5$/CdS/*N*,*N*′-(1,4-phenylene) bispyridinium ditriflate	Monochromatic LED (450 nm, 65 mW·cm^{-2}), 0.1 M $KHCO_3$	CO at 0 V vs RHE, 2 h	The molecular additive resulted in lower coarsening and improved retention of the CdS coating	[220]
CIGS/TiO_2/Co-qPyH	150 W Xe lamp, 0.1 M $KHCO_3$	CO (97% selectivity) at −0.06 V vs RHE, 2 h	Photocurrent showed only a slight decay after 2 h electrolysis	[221]
CIGS/CdS/ZnO/AZO	300 W Xe arc lamp, 0.5 M $KHCO_3$	CO (FE: 99.3%) at −0.2 V vs RHE; CO (49.3%), HCOOH (15.4%), CH_3OH (8.45%) at −0.5 V vs RHE	—	[222]
CZTS/[RuCE + RuCA]	Xe light source, purified water	$HCOO^-$ (FE: 82%) at −0.4 V vs RHE, 3 h	—	[223]
CZTS/CdS	Solar simulator (100 mW·cm^{-2}), 0.1 M $KHCO_3$	CO, CH_3OH, C_2H_5OH (measured at −0.4, −0.5, −0.6, −0.7, and −0.8 V vs RHE)	—	[224]
$Zn_{0.5}Cu_2ZnGeS_4$	Solar simulator, 0.1 M $KHCO_3$	CO (FE: 3.3%) at −0.2 V vs RHE, 2 h	—	[225]

FE, Faradaic efficiency.

(compared to 5.1% for bare $CuFe_2O_4$) as well as a higher selectivity for methanol formation, 72, 87, and 73%, respectively (compared to 62% for bare $CuFe_2O_4$). This improvement was attributed to an enhanced electron-hole separation and to an increased CO_2 adsorption for the case of PANI. A direct Z-scheme system of $Cu_2V_2O_7$ (with a band gap of 2.01 eV) and g-C_3N_4 was devised [201]. Under illumination of light with wavelength of 400–700 nm, the $Cu_2V_2O_7$/g-C_3N_4 system produced a much higher photocurrent response than $Cu_2V_2O_7$ or g-C_3N_4 alone. CO_2 photoreduction (under a photocatalytic scheme) resulted in the formation of CH_4, CO, and O_2 with rates of 305, 166, and 706 $\mu mol \cdot g^{-1}$ catalyst$\cdot h^{-1}$, respectively. $CuNb_2O_6$, belonging to a class of metal niobates with an orthorhombic columbite structure, was found to be photoactive for PEC CO_2 reduction even without any co-catalyst [202]. It showed photoresponse under visible light illumination (150 W tungsten-halogen lamp), consistent with its optical band gap of 1.77 eV. Photocurrents measured in CO_2-saturated 0.1 M $NaHCO_3$ solution (pH 7) were up to six times greater than those measured in an N_2-saturated 0.1 M Na_2SO_4 solution (pH 7), indicating that the photocurrent was being used in the reduction of CO_2, although no efforts were done to identify and quantify the reduction products. Another copper niobate, $Cu_3Nb_2O_8$ (with band gap of 2.5 eV), was also found to photoelectrochemically reduce CO_2 under AM 1.5 G illumination, with CO as the primary product [203]. However, the Faradaic efficiency for CO evolution was found to be around 9% (at −0.20 V vs Ag/AgCl), indicating that majority of the cathodic photocurrent was being used in the photocorrosion of the $Cu_3Nb_2O_8$ film. Indeed, chronoamperometry tests (in CO_2-saturated 0.5 M $NaHCO_3$ solution at −0.20 V vs Ag/AgCl) showed a 98% decrease in the initial photocurrent only after 20 min. Reannealing of the tested films restored the initial photocurrent to that of the as-synthesized film, corroborating the cathodic photocorrosion of $Cu_3Nb_2O_8$, and the use of protective layers or addition of co-catalysts will be needed to improve its PEC performance.

The results of PEC CO_2 reduction studies on the copper ternary oxides, where the reduction products were identified and quantified, are summarized in Table 3. Although beyond the scope of this review, there are many research efforts in recent years to explore other classes of materials as photocathodes. Non-copper ternary oxides, such as $AgRhO_2$ [204], $BiFeO_3$ [205,206], $CaFe_2O_4$ [207,208], $Ca_2Fe_2O_5$ [209,210], $LaFeO_3$ [211,212], $NiFeO_4$ [213], and $PbMoO_4$ [214], have been prepared as photocathodes but their application towards PEC CO_2 reduction is yet to be investigated. On the other hand, copper-based chalcogenides, such as $CuInS_2$ [215–218], $CuGaS_2$ [219], $CuGa_3Se_5$ [220], $Cu(In,Ga)Se_2$ [221,222], Cu_2ZnSnS_4 [223,224], and Cu_2ZnGeS_4 [225], which have been widely used in solar cells due to their favorable transport properties, have recently been investigated as CO_2 reduction photocathodes (Table 4). Although their efficiency and stability are comparable with the copper ternary oxides, the cost and toxicity (primarily of In and Ga), as well as the complicated preparation methods that limit possibilities for scale-up, are major issues that need to be addressed [226].

4 Summary and outlook

In the search for new p-type materials suitable as photocathode for PEC applications, copper ternary oxides have recently gained attention due to their favorable band structure and earth-abundant nature. This article examined the current progress achieved with $CuFeO_2$ and $CuBi_2O_4$ by summarizing the various strategies to improve their efficiency and stability towards CO_2 reduction. Other copper ternary oxides, $CuCrO_2$, $CuGaO_2$, $CuFe_2O_4$, $Cu_2V_2O_7$, $CuNb_2O_6$, and $Cu_3Nb_2O_8$, were also reviewed. For these photocathodes, CO, HCOOH, HCOH, CH_3OH, and CH_4 as well as C_2H_5OH and $(CH_3)_2CO$ were the observed CO_2 reduction products (Table 3). However, photocorrosion is still significant in these materials. Several studies are in search of selective inhibitors that can allow only specific reactions to proceed, aiding the overall kinetics. Polymers and membranes have been used recently as the protective overlayer that simultaneously fosters CO_2 binding sites [227] and modifies the surface hydrophobicity to improve selectivity [228].

Most of the papers reviewed here approach the improvement in the copper oxide photocathodes from the viewpoint of charge transport. In Cu_2O, it has been observed that surface recombination and bulk transport were the contributors to the lifetime of charges [229]. A close connection between semiconductor and conducting support leads to faster charge separation; the challenge is to determine the type and structure of the support and the copper oxides. However, a system of efficient and stable CO_2 reduction relies not only on charge transport but also on chemical reaction kinetics and mass transfer of reactants and products. Theoretical studies on CO_2 adsorption and reaction mechanisms are being done by several groups [230,231]. Similarly, there have also been theoretical and experimental works to understand CO_2 reduction active sites in copper and copper-based semiconductors [228,232]. Studies such as these can guide synthesis of structures with complementary adsorption and active site.

It remains a prospect whether a semiconductor material with the correct compositional mix that satisfies all

requirements as photoelectrode can be identified. More likely, this semiconductor will come from complex metal oxides where there are greater possibilities for tuning and optimization of material properties. With this large material space, theory on interfacial phenomena, such as CO_2 activation and intermediates, should be refined much further to establish advanced descriptors for computational screening of new complex oxides. High throughput methodologies for the synthesis of a large library of candidate materials and testing of their relevant properties for PEC applications will further accelerate materials discovery. It must be noted, however, that with increasing complexity of multinary oxides, the cost and ease of processability, along with sustainability considerations critical towards large scale production, become more difficult to attain.

In the past few decades, significant achievements have been made in the field of PEC solar fuel generation. At its current state, further advances will rely not only on materials development, but also on device modeling and simulation and techno-economic analysis. For PEC CO_2 reduction to become a viable, carbon-neutral technology that can harness the enormous, undeveloped potential of solar energy, many key challenges remain to be solved.

Funding information: This work was supported by the Engineering Research and Development for Technology (ERDT) of the Department of Science and Technology (DOST).

Author contributions: I.L.E. Gonzaga: conceptualization and writing – original draft, review & editing; C.C. Mercado: conceptualization, writing – review & editing, and supervision.

Conflict of interest: Authors state no conflict of interest.

References

[1] Lewis, N. and D. Nocera. Powering the planet: Chemical challenges in solar energy utilization. *Proceedings of the National Academy of Sciences*, Vol. 103, No. 43, 2006, pp. 15729–15735.

[2] Pleskov, Y. Solar energy conversion in photoelectrochemical cells with semiconductor electrodes. *Progress in Surface Science*, Vol. 15, No. 4, 1984, pp. 401–456.

[3] Lewis, N. Research opportunities to advance solar energy utilization. *Science*, Vol. 351, No. 6271, 2016, id. aad1920.

[4] Centi, G. and S. Perathoner. Towards solar fuels from water and CO_2. *Chemsuschem*, Vol. 3, No. 2, 2010, pp. 195–208.

[5] Yan, Y., J. Gu, E. L. Zeitler, and A. B. Bocarsly. Photoelectrocatalytic reduction of carbon dioxide. In *Carbon dioxide utilization: Closing the carbon cycle*, 1st edn, Styring, P., A. Quadrelli, and K. Armstrong, Eds, Elsevier Inc., Amsterdam, The Netherlands, 2015, pp. 211–233.

[6] Tilley, S. D. Recent advances and emerging trends in photoelectrochemical solar energy conversion. *Advanced Energy Materials*, Vol. 9, No. 2, 2019, id. 1802877.

[7] Gust, D., T. Moore, and A. Moore. Solar fuels via artificial photosynthesis. *Accounts of Chemical Research*, Vol. 42, No. 12, 2009, pp. 1890–1898.

[8] Roy, S., O. Varghese, M. Paulose, and C. Grimes. Toward solar fuels: Photocatalytic conversion of carbon dioxide to hydrocarbons. *ACS Nano*, Vol. 4, No. 3, 2010, pp. 1259–1278.

[9] Hoffmann, M., J. Moss, and M. Baum. Artificial photosynthesis: semiconductor photocatalytic fixation of CO_2 to afford higher organic compounds. *Dalton Transactions*, Vol. 40, No. 19, 2011, pp. 5151–5158.

[10] Barber, J. and P. Tran. From natural to artificial photosynthesis. *Journal of The Royal Society Interface*, Vol. 10, No. 81, 2013, id. 20120984.

[11] Krol, R. and M. Grätzel. *Photoelectrochemical hydrogen production*. Springer, New York, NY, 2012.

[12] Olah, G., G. Prakash, and A. Goeppert. Anthropogenic chemical carbon cycle for a sustainable future. *Journal of The American Chemical Society*, Vol. 133, No. 33, 2011, pp. 12881–12898.

[13] Spinner, N., J. Vega, and W. Mustain. Recent progress in the electrochemical conversion and utilization of CO_2. *Catalysis Science & Technology*, Vol. 2, No. 1, 2012, pp. 19–28.

[14] White, J., M. Baruch, J. Pander, Y. Hu, I. Fortmeyer, J. Park, et al. Light-driven heterogeneous reduction of carbon dioxide: photocatalysts and photoelectrodes. *Chemical Reviews*, Vol. 115, No. 23, 2015, pp. 12888–12935.

[15] Montoya, J., L. Seitz, P. Chakthranont, A. Vojvodic, T. Jaramillo, and J. Nørskov. Materials for solar fuels and chemicals. *Nature Materials*, Vol. 16, No. 1, 2016, pp. 70–81.

[16] Kumaravel, V., J. Bartlett, and S. Pillai. Photoelectrochemical conversion of carbon dioxide (CO_2) into fuels and value-added products. *ACS Energy Letters*, Vol. 5, No. 2, 2020, pp. 486–519.

[17] Mikkelsen, M., M. Jørgensen, and F. C. Krebs. The teraton challenge. A review of fixation and transformation of carbon dioxide. *Energy & Environmental Science*, Vol. 3, No. 1, 2010, pp. 43–81.

[18] Greenblatt, J., D. Miller, J. Ager, F. Houle, and J. Sharp. The technical and energetic challenges of separating (photo) electrochemical carbon dioxide reduction products. *Joule*, Vol. 2, No. 3, 2018, pp. 381–420.

[19] Freund, H-J. and M. W. Roberts. Surface chemistry of carbon dioxide. *Surface Science Reports*, Vol. 25, No. 8, 1996, pp. 225–273.

[20] Kumar, B., M. Llorente, J. Froehlich, T. Dang, A. Sathrum, and C. P. Kubiak. Photochemical and photoelectrochemical reduction of CO_2. *Annual Review of Physical Chemistry*, Vol. 63, 2012, pp. 541–569.

[21] Aresta, M. and A. Angelini. The carbon dioxide molecule and the effects of its interaction with electrophiles and nucleophiles. In *Carbon dioxide and organometallics*, Lu X. B., ed., Springer, Cham, 2016, pp. 1–38.

[22] Costentin, C., M. Robert, and J-M. Savéant. Catalysis of the electrochemical reduction of carbon dioxide. *Chemical Society Reviews*, Vol. 42, No. 6, 2013, pp. 2423–2436.

[23] Dodson, L. G., M. C. Thompson, and J. M. Weber. Characterization of intermediate oxidation states in CO_2 activation. *Annual Review of Physical Chemistry*, Vol. 69, 2018, pp. 231–252.
[24] Álvarez, A., M. Borges, J. J. Corral-Pérez, J. G. Olcina, L. Hu, D. Cornu, et al. CO_2 activation over catalytic surfaces. *ChemPhysChem*, Vol. 18, No. 22, 2017, pp. 3135–3141.
[25] Habisreutinger, S., L. Schmidt-Mende, and J. Stolarczyk. Photocatalytic reduction of CO_2 on TiO_2 and other semiconductors. *Angewandte Chemie International Edition*, Vol. 52, No. 29, 2013, pp. 7372–7408.
[26] Peng, C., G. Reid, H. Wang, and P. Hu. Perspective: photocatalytic reduction of CO_2 to solar fuels over semiconductors. *The Journal of Chemical Physics*, Vol. 147, No. 3, 2017, id. 030901.
[27] Stolarczyk, J. K., S. Bhattacharyya, L. Polavarapu, and J. Feldmann. Challenges and prospects in solar water splitting and CO_2 reduction with inorganic and hybrid nanostructures. *ACS Catalysis*, Vol. 8, No. 4, 2018, pp. 3602–3635.
[28] Du, C., X. Wang, W. Chen, S. Feng, J. Wen, and Y. A. Wu. CO_2 transformation to multicarbon products by photocatalysis and electrocatalysis. *Materials Today Advances*, Vol. 6, 2020, id. 100071.
[29] Liu, Y. and L. Guo. On factors limiting the performance of photoelectrochemical CO_2 reduction. *The Journal of Chemical Physics*, Vol. 152, No. 10, 2020, id. 100901.
[30] Butler, M. A. and D. S. Ginley. Principles of photoelectrochemical, solar energy conversion. *Journal of Materials Science*, Vol. 15, No. 1, 1980, pp. 1–19.
[31] Lewis, N. S. and G. A. Shreve. Photochemical and photoelectrochemical reduction of carbon dioxide. In *Electrochemical and electrocatalytic reactions of carbon dioxide*, Sullivan, B. P., K. Krist, and H. E. Guard, Eds, Elsevier Inc., Amsterdam, The Netherlands, 1993, pp. 263–289.
[32] Cole, E. B. and A. B. Bocarsly. Photochemical, electrochemical, and photoelectrochemical reduction of carbon dioxide. In *Carbon dioxide as chemical feedstock*, M. Aresta, Ed, John Wiley & Sons, Ltd, WILEY-VCH Verlag GmbH & Co., KGaA, Weinheim, Germany, 2010, pp. 291–316.
[33] Guijarro, N., M. S. Prévot, and K. Sivula. Surface modification of semiconductor photoelectrodes. *Physical Chemistry Chemical Physics*, Vol. 17, No. 24, 2015, pp. 15655–15674.
[34] Li, J. and N. Wu. Semiconductor-based photocatalysts and photoelectrochemical cells for solar fuel generation: a review. *Catalysis Science & Technology*, Vol. 5, No. 3, 2015, pp. 1360–1384.
[35] Sivula, K. and R. van de Krol. Semiconducting materials for photoelectrochemical energy conversion. *Nature Reviews Materials*, Vol. 1, No. 2, 2016, pp. 1–16.
[36] Tu, W., Y. Zhou, and Z. Zou. Photocatalytic conversion of CO_2 into renewable hydrocarbon fuels: state-of-the-art accomplishment, challenges, and prospects. *Advanced Materials*, Vol. 26, No. 27, 2014, pp. 4607–4626.
[37] Marszewski, M., S. Cao, J. Yu, and M. Jaroniec. Semiconductor-based photocatalytic CO_2 conversion. *Materials Horizons*, Vol. 2, No. 3, 2015, pp. 261–278.
[38] Xie, S., Q. Zhang, G. Liu, and Y. Wang. Photocatalytic and photoelectrocatalytic reduction of CO_2 using heterogeneous catalysts with controlled nanostructures. *Chemical Communications*, Vol. 52, No. 1, 2016, pp. 35–59.
[39] Vu, N., S. Kaliaguine, and T. Do. Critical aspects and recent advances in structural engineering of photocatalysts for sunlight-driven photocatalytic reduction of CO_2 into fuels. *Advanced Functional Materials*, Vol. 29, No. 31, 2019, id. 1901825.
[40] Ding, P., T. Jiang, N. Han, and Y. Li. Photocathode engineering for efficient photoelectrochemical CO_2 reduction. *Materials Today Nano*, Vol. 10, 2020, id. 100077.
[41] Chen, P., Y. Zhang, Y. Zhou, and F. Dong. Photoelectrocatalytic carbon dioxide reduction: fundamental, advances and challenges. *Nano Materials Science*, Vol. 3, No. 4, 2021, pp. 344–367.
[42] Rajeshwar, K., P. A. Maggard, and S. O'Donnell. In search of the "perfect" inorganic semiconductor/liquid interface for solar water splitting. *The Electrochemical Society Interface*, Vol. 30, No. 1, 2021, pp. 47–51.
[43] Wick, R. and D. D. Tilley. Photovoltaic and photoelectrochemical solar energy conversion with Cu_2O. *The Journal of Physical Chemistry C*, Vol. 119, No. 47, 2015, pp. 26243–26257.
[44] Moakhar, R. S., S. M. Hosseini-Hosseinabad, S. Masudy-Panah, A. Seza, M. Jalali, H. Fallah-Arani, et al. Photoelectrochemical water-splitting using CuO-based electrodes for hydrogen production: a review. *Advanced Materials*, Vol. 33, No. 33, 2021, id. 2007285.
[45] Sullivan, I., B. Zoellner, and P. A. Maggard. Copper(I)-based p-type oxides for photoelectrochemical and photovoltaic solar energy conversion. *Chemistry of Materials*, Vol. 28, No. 17, 2016, pp. 5999–6016.
[46] Lumley, M. A., A. Radmilovic, Y. J. Jang, A. E. Lindberg, and K. S. Choi. Perspectives on the development of oxide-based photocathodes for solar fuel production. *Journal of The American Chemical Society*, Vol. 141, No. 46, 2019, pp. 18358–18369.
[47] Li, C., J. He, Y. Xiao, Y. Li, and J-J. Delaunay. Earth-abundant Cu-based metal oxide photocathodes for photoelectrochemical water splitting. *Energy & Environmental Science*, Vol. 13, No. 10, 2020, pp. 3269–3306.
[48] Wang, K., Y. Ma, Y. Liu, W. Qiu, Q. Wang, X. Yang, et al. Insights into the development of Cu-based photocathodes for carbon dioxide (CO_2) conversion. *Green Chemistry*, Vol. 23, No. 9, 2021, pp. 3207–3240.
[49] Abdi, F. F. and S. P. Berglund. Recent developments in complex metal oxide photoelectrodes. *Journal of Physics D: Applied Physics*, Vol. 50, No. 19, 2017, id. 193002.
[50] Rajeshwar, K., M. K. Hossain, R. T. Macaluso, C. Janáky, A. Varga, and P. J. Kulesza. Review – Copper oxide-based ternary and quaternary oxides: where solid-state chemistry meets photoelectrochemistry. *Journal of The Electrochemical Society*, Vol. 165, No. 4, 2018, pp. H3192–H3206.
[51] He, H., A. Liao, W. Guo, W. Luo, Y. Zhou, and Z. Zou. State-of-the-art progress in the use of ternary metal oxides as photoelectrode materials for water splitting and organic synthesis. *Nano Today*, Vol. 28, 2019, id. 100763.
[52] Gerischer, H. Electrochemical behavior of semiconductors under illumination. *Journal of The Electrochemical Society*, Vol. 113, No. 11, 1966, id. 1174.

[53] Bard, A. Photoelectrochemistry and heterogeneous photocatalysis at semiconductors. *Journal of Photochemistry*, Vol. 10, No. 1, 1979, pp. 59–75.
[54] Memming, R. Solar energy conversion by photoelectrochemical processes. *Electrochimica Acta*, Vol. 25, No. 1, 1980, pp. 77–88.
[55] Chang, X., T. Wang, P. Yang, G. Zhang, and J. Gong. The development of cocatalysts for photoelectrochemical CO_2 reduction. *Advanced Materials*, Vol. 31, No. 31, 2019, id. 1804710.
[56] Gurevich, Y. Y. and Y. V. Pleskov. Photoelectrochemistry of semiconductors. *Elsevier – Semiconductors and Semimetals*, Vol. 19, 1983, pp. 255–328.
[57] Nozik, A. J. and R. Memming. Physical chemistry of semiconductor – liquid interfaces. *The Journal of Physical Chemistry*, Vol. 100, No. 31, 1996, pp. 13061–13078.
[58] Boston, D., K. L. Huang, N. de Tacconi, N. Myung, F. Macdonell, and K. Rajeshwar. Electro-and photocatalytic reduction of CO_2: The homogeneous and heterogeneous worlds collide? In *Photoelectrochemical water splitting: materials, processes and architectures*, Lewerenz, H-J. and L. Peter, Eds, The Royal Society of Chemistry, Cambridge, UK, 2013, pp. 289–332.
[59] Rajeshwar, K., A. Thomas, and C. Janáky. Photocatalytic activity of inorganic semiconductor surfaces: myths, hype, and reality. *The Journal of Physical Chemistry Letters*, Vol. 6, No. 1, 2015, pp. 139–147.
[60] Barton, E., D. Rampulla, and A. Bocarsly. Selective solar-driven reduction of CO_2 to methanol using a catalyzed p-GaP based photoelectrochemical cell. *Journal of The American Chemical Society*, Vol. 130, No. 20, 2008, pp. 6342–6344.
[61] Ghadimkhani, G., N. R. de Tacconi, W. Chanmanee, C. Janaky, and K. Rajeshwar. Efficient solar photoelectrosynthesis of methanol from carbon dioxide using hybrid CuO–Cu_2O semiconductor nanorod arrays. *Chemical Communications*, Vol. 49, No. 13, 2013, pp. 1297–1299.
[62] Halmann, M. Photoelectrochemical reduction of aqueous carbon dioxide on p-type gallium phosphide in liquid junction solar cells. *Nature*, Vol. 275, No. 5676, 1978, pp. 115–116.
[63] Aurian-Blajeni, B., M. Halmann, and J. Manassen. Electrochemical measurement on the photoelectrochemical reduction of aqueous carbon dioxide on p-Gallium phosphide and p-Gallium arsenide semiconductor electrodes. *Solar Energy Materials*, Vol. 8, No. 4, 1983, pp. 425–440.
[64] Ito, K., S. Ikeda, M. Yoshida, S. Ohta, and T. Iida. On the reduction products of carbon dioxide at a p-type gallium phosphide photocathode in aqueous electrolytes. *Bulletin of the Chemical Society of Japan*, Vol. 57, No. 2, 1984, pp. 583–584.
[65] Ikeda, S., A. Yamamoto, H. Noda, M. Maeda, and K. Ito. Influence of surface treatment of the p-GaP photocathode on the photoelectrochemical reduction of carbon dioxide. *Bulletin of the Chemical Society of Japan*, Vol. 66, No. 9, 1993, pp. 2473–2477.
[66] Hirota, K., D. A. Tryk, T. Yamamoto, K. Hashimoto, M. Okawa, and A. Fujishima. Photoelectrochemical reduction of CO_2 in a high-pressure CO_2^+ methanol medium at p-type semiconductor electrodes. *The Journal of Physical Chemistry B*, Vol. 102, No. 49, 1998, pp. 9834–9843.
[67] Canfield, D. and K. W. Frese Jr. Reduction of carbon dioxide to methanol on n- and p-GaAs and p-InP. Effect of crystal face, electrolyte and current density. *Journal of the Electrochemical Society*, Vol. 130, No. 8, 1983, pp. 1772–1773.
[68] Zafrir, M., M. Ulman, Y. Zuckerman, and Halmann. Photoelectrochemical reduction of carbon dioxide to formic acid, formaldehyde and methanol on p-gallium arsenide in an aqueous V(II)-V(III) chloride redox system. *Journal of Electroanalytical Chemistry and Interfacial Electrochemistry*, Vol. 159, No. 2, 1983, pp. 373–389.
[69] Sears, W. M. and S. R. Morrison. Carbon dioxide reduction on gallium arsenide electrodes. *The Journal of Physical Chemistry*, Vol. 89, No. 15, 1985, pp. 3295–3298.
[70] Yoneyama, R., K. Sigumura, and S. Kuwabata. Effects of electrolytes on the photoelectrochemical reduction of carbon dioxide at illuminated p-type cadmium telluride and p-type indium phosphide electrodes in aqueous solutions. *Journal of Electroanalytical Chemistry and Interfacial Electrochemistry*, Vol. 249, 1988, pp. 143–153.
[71] Hirota, K., D. A. Tryk, K. Hashimoto, M. Okawa, and A. Fujishima. Photoelectrochemical reduction of CO_2 at high current densities at p-InP electrodes. *Journal of The Electrochemical Society*, Vol. 145, No. 5, 1998, pp. L82–L84.
[72] Aurian-Blajeni, B., M. A. Habib, I. Taniguchi, and J. O. Bockris. The study of adsorbed species during the photoassisted reduction of carbon dioxide at a p-CdTe electrode. *Journal of Electroanalytical Chemistry and Interfacial Electrochemistry*, Vol. 157, No. 2, 1983, pp. 399–404.
[73] Taniguchi, I., B. Aurian-Blajeni, and J. O. Bockris. Photo-aided reduction of carbon dioxide to carbon monoxide. *Journal of Electroanalytical Chemistry and Interfacial Electrochemistry*, Vol. 157, No. 1, 1983, pp. 179–182.
[74] Taniguchi, I., B. Aurian-Blajeni, and J. O. Bockris. The reduction of carbon dioxide at illuminated p-type semiconductor electrodes in nonaqueous media. *Electrochimica Acta*, Vol. 29, No. 7, 1984, pp. 923–932.
[75] Junfu, L. and C. Baozhu. Photoelectrochemical reduction of carbon dioxide on a p+/p–Si photocathode in aqueous electrolyte. *Journal of Electroanalytical Chemistry*, Vol. 324, No. 1–2, 1992, pp. 191–200.
[76] Ikeda, S., M. Yoshida, and K. Ito. Photoelectrochemical reduction products of carbon dioxide at metal coated p-GaP photocathodes in aqueous electrolytes. *Bulletin of The Chemical Society of Japan*, Vol. 58, No. 5, 1985, pp. 1353–1357.
[77] Hinogami, R., Y. Nakamura, S. Yae, and Y. Nakato. An approach to ideal semiconductor electrodes for efficient photoelectrochemical reduction of carbon dioxide by modification with small metal particles. *The Journal of Physical Chemistry B*, Vol. 102, No. 6, 1998, pp. 974–980.
[78] Kaneco, S., H. Katsumata, T. Suzuki, and K. Ohta. Photoelectrocatalytic reduction of CO_2 in LiOH/methanol at metal-modified p-InP electrodes. *Applied Catalysis B: Environmental*, Vol. 64, No. 1–2, 2006, pp. 139–145.
[79] Hinogami, R., T. Mori, S. Yae, and Y. Nakato. Efficient photoelectrochemical reduction of carbon dioxide on a p-type silicon (p-Si) electrode modified with very small copper particles. *Chemistry Letters*, Vol. 23, No. 9, 1994, pp. 1725–1728.

[80] Aurian-Blajeni, B., I. Taniguchi, and J. O. Bockris. Photoelectrochemical reduction of carbon dioxide using polyaniline-coated silicon. *Journal of Electroanalytical Chemistry and Interfacial Electrochemistry*, Vol. 149, No. 1–2, 1983, pp. 291–293.

[81] Daube, K. A., D. J. Harrison, T. E. Mallouk, A. J. Ricco, S. Chao, M. S. Wrighton, et al. Electrode-confined catalyst systems for use in optical-to-chemical energy conversion. *Journal of Photochemistry*, Vol. 29, No. 1–2, 1985, pp. 71–88.

[82] Taniguchi, Y., H. Yoneyama, and H. Tamura. Photoelectrochemical reduction of carbon dioxide at p-type gallium phosphide electrodes in the presence of crown ether. *Bulletin of The Chemical Society of Japan*, Vol. 55, No. 7, 1982, pp. 2034–2039.

[83] Parkinson, B. A. and P. F. Weaver. Photoelectrochemical pumping of enzymatic CO_2 reduction. *Nature*, Vol. 309, No. 5964, 1984, pp. 148–149.

[84] Beley, M., J. P. Collin, J. P. Sauvage, J. P. Petit, and P. Chartier. Photoassisted electro-reduction of CO_2 on p-GaAs in the presence of Ni cyclam^{2+}. *Journal of Electroanalytical Chemistry and Interfacial Electrochemistry*, Vol. 206, No. 1–2, 1986, pp. 333–339.

[85] Bockris, J. O. and J. C. Wass. The photoelectrocatalytic reduction of carbon dioxide. *Journal of The Electrochemical Society*, Vol. 136, No. 9, 1989, pp. 2521–2528.

[86] Petit, J. P., P. Chartier, M. Beley, and J. P. Deville. Molecular catalysts in photoelectrochemical cells. *Journal of Electroanalytical Chemistry and Interfacial Electrochemistry*, Vol. 269, No. 2, 1989, pp. 267–281.

[87] Lany, S. Semiconducting transition metal oxides. *Journal of Physics: Condensed Matter*, Vol. 27, No. 28, 2015, id. 283203.

[88] Monllor-Satoca, D., M. I. Díez-García, T. Lana-Villarreal, and R. Gómez. Photoelectrocatalytic production of solar fuels with semiconductor oxides: materials, activity and modeling. *Chemical Communications*, Vol. 56, No. 82, 2020, pp. 12272–12289.

[89] Rao, C. N. R. Transition metal oxides. *Annual Review of Physical Chemistry*, Vol. 40, No. 1, 1989, pp. 291–326.

[90] Cox, P. A. *Transition metal oxides: An introduction to their electronic structure and properties*. Oxford University Press, New York, United States, 2010.

[91] Inoue, T., A. Fujishima, S. Konishi, and K. Honda. Photoelectrocatalytic reduction of carbon dioxide in aqueous suspensions of semiconductor powders. *Nature*, Vol. 277, No. 5698, 1979, pp. 637–638.

[92] Rajeshwar, K. Solar energy conversion and environmental remediation using inorganic semiconductor–liquid interfaces: the road traveled and the way forward. *The Journal of Physical Chemistry Letters*, Vol. 2, No. 11, 2011, pp. 1301–1309.

[93] Hautier, G., A. Miglio, G. Ceder, G. M. Rignanese, and X. Gonze. Identification and design principles of low hole effective mass p-type transparent conducting oxides. *Nature Communications*, Vol. 4, No. 1, 2013, pp. 1–7.

[94] Luo, J., L. Steier, M. K. Son, M. Schreier, M. T. Mayer, and M. Grätzel. Cu_2O nanowire photocathodes for efficient and durable solar water splitting. *Nano Letters*, Vol. 16, No. 3, 2016, pp. 1848–1857.

[95] Jang, Y. J., J. W. Jang, S. H. Choi, J. Y. Kim, J. H. Kim, D. H. Youn, et al. Tree branch-shaped cupric oxide for highly effective photoelectrochemical water reduction. *Nanoscale*, Vol. 7, No. 17, 2015, pp. 7624–7631.

[96] Cardiel, A. C., K. J. McDonald, and K. S. Choi. Electrochemical growth of copper hydroxy double salt films and their conversion to nanostructured p-type CuO photocathodes. *Langmuir*, Vol. 33, No. 37, 2017, pp. 9262–9270.

[97] Tilley, S. D., M. Schreier, J. Azevedo, M. Stefik, and M. Graetzel. Ruthenium oxide hydrogen evolution catalysis on composite cuprous oxide water-splitting photocathodes. *Advanced Functional Materials*, Vol. 24, No. 3, 2013, pp. 303–311.

[98] Morales-Guio, C. G., S. D. Tilley, H. Vrubel, M. Grätzel, and X. Hu. Hydrogen evolution from a copper(I) oxide photocathode coated with an amorphous molybdenum sulphide catalyst. *Nature Communications*, Vol. 5, No. 1, 2014, pp. 1–7.

[99] Won, D. H., C. H. Choi, J. Chung, and S. I. Woo. Photoelectrochemical production of formic acid and methanol from carbon dioxide on metal-decorated CuO/Cu_2O-layered thin films under visible light irradiation. *Applied Catalysis B: Environmental*, Vol. 158–159, 2014, pp. 217–223.

[100] de Brito, J. F., A. R. Araujo, K. Rajeshwar, and M. V. B. Zanoni. Photoelectrochemical reduction of CO_2 and Cu/Cu_2O films: product distribution and pH effects. *Chemical Engineering Journal*, Vol. 264, 2015, pp. 302–309.

[101] Schreier, M., P. Gao, M. T. Mayer, J. Luo, T. Moehl, M. K. Nazeeruddin, et al. Efficient and selective carbon dioxide reduction on low cost protected Cu_2O photocathodes using a molecular catalyst. *Energy & Environmental Science*, Vol. 8, No. 3, 2015, pp. 855–861.

[102] Schreier, M., J. Luo, P. Gao, T. Moehl, M. T. Mayer, and M. Grätzel. Covalent immobilization of a molecular catalyst on Cu_2O photocathodes for CO reduction. *Journal of The American Chemical Society*, Vol. 138, No. 6, 2016, pp. 1938–1946.

[103] Landaeta, E., R. A. Masitas, T. B. Clarke, S. Rafacz, D. A. Nelson, M. Isaacs, et al. Copper-oxide-coated silver nanodendrites for photoelectrocatalytic CO_2 reduction to acetate at low overpotential. *ACS Applied Nano Materials*, Vol. 3, No. 4, 2020, pp. 3478–3486.

[104] Paracchino, A., V. Laporte, K. Sivula, M. Grätzel, and E. Thimsen. Highly active oxide photocathode for photoelectrochemical water reduction. *Nature Materials*, Vol. 10, No. 6, 2011, pp. 456–461.

[105] Azevedo, J., S. D. Tilley, M. Schreier, M. Stefik, C. Sousa, J. P. Araújo, et al. Tin oxide as stable protective layer for composite cuprous oxide water-splitting photocathodes. *Nano Energy*, Vol. 24, 2016, pp. 10–16.

[106] Lee, K., S. Lee, H. Cho, S. Jeong, W. D. Kim, S. Lee, et al. Cu^+-incorporated TiO_2 overlayer on Cu_2O nanowire photocathodes for enhanced photoelectrochemical conversion of CO_2 to methanol. *Journal of Energy Chemistry*, Vol. 27, No. 1, 2018, pp. 264–270.

[107] Deng, X., R. Li, S. Wu, L. Wang, J. Hu, J. Ma, et al. Metal–organic framework coating enhances the performance of Cu_2O in photoelectrochemical CO_2 reduction. *Journal of The American Chemical Society*, Vol. 141, No. 27, 2019, pp. 10924–10929.

[108] Li, P., H. Wang, J. Xu, H. Jing, J. Zhang, H. Han, et al. Reduction of CO_2 to low carbon alcohols on CuO FCs/Fe_2O_3 NTs catalyst with photoelectric dual catalytic interfaces. *Nanoscale*, Vol. 5, No. 23, 2013, pp. 11748–11754.

[109] Kecsenovity, E., B. Endrődi, Z. Pápa, K. Hernádi, K. Rajeshwar, and C. Janáky. Decoration of ultra-long carbon nanotubes with Cu_2O nanocrystals: a hybrid platform for enhanced photoelectrochemical CO_2 reduction. *Journal of Materials Chemistry A*, Vol. 4, No. 8, 2016, pp. 3139–3147.

[110] de Brito, J. F. and M. V. B. Zanoni. On the application of Ti/TiO_2/CuO n-p junction semiconductor: a case study of electrolyte, temperature and potential influence on CO_2 reduction. *Chemical Engineering Journal*, Vol. 318, 2017, pp. 264–271.

[111] Septina, W., R. R. Prabhakar, R. Wick, T. Moehl, and S. D. Tilley. Stabilized solar hydrogen production with CuO/CdS heterojunction thin film photocathodes. *Chemistry of Materials*, Vol. 29, No. 4, 2017, pp. 1735–1743.

[112] Li, J. M., C. W. Tsao, M. J. Fang, C. C. Chen, C. W. Liu, and Y. J. Hsu. TiO_2-Au-Cu_2O photocathodes: Au-mediated Z-scheme charge transfer for efficient solar-driven photoelectrochemical reduction. *ACS Applied Nano Materials*, Vol. 1, No. 12, 2018, pp. 6843–6853.

[113] Jiang, X. X., X. D. Hu, M. Tarek, P. Saravanan, R. Alqadhi, S. Y. Chin, et al. Tailoring the properties of g-C_3N_4 with CuO for enhanced photoelectrocatalytic CO_2 reduction to methanol. *Journal of CO_2 Utilization*, Vol. 40, 2020, id. 101222.

[114] Tarek, M., K. M. R. Karim, S. Sarmin, H. R. Ong, H. Abdullah, C. K. Cheng, et al. Photoelectrochemical activity of CuO-CdS heterostructured catalyst for CO_2 reduction. In *IOP Conference Series: Materials Science and Engineering*, Vol. 736, No. 4, 2020, id. 042023.

[115] Xing, H., E. Lei, Z. Guo, D. Zhao, and Z. Liu. Enhancement in the charge transport and photocorrosion stability of CuO photocathode: the synergistic effect of spatially separated dual-cocatalysts and p-n heterojunction. *Chemical Engineering Journal*, Vol. 394, 2020, id. 124907.

[116] Bienkowski, K., A. Małolepszy, L. Stobiński, M. Strawski, P. Wróbel, and R. Solarska. Influence of Fermi-level engineering in multi-interface CuO/Cu_2O||rGO||h-WO_3||rGO|| photoelectrodes on photoelectrochemical CO_2 reduction. *Energy Technology*, Vol. 10, 2022, id. 2100999.

[117] Bosman, A. and H. van Daal. Small-polaron versus band conduction in some transition-metal oxides. *Advances in Physics*, Vol. 19, No. 77, 1970, pp. 1–117.

[118] Rettie, A. J. E., W. D. Chemelewski, D. Emin, and C. B. Mullins. Unravelling small-polaron transport in metal oxide photoelectrodes. *The Journal of Physical Chemistry Letters*, Vol. 7, No. 3, 2016, pp. 471–479.

[119] Marquardt, M. A., N. A. Ashmore, and D. P. Cann. Crystal chemistry and electrical properties of the delafossite structure. *Thin Solid Films*, Vol. 496, No. 1, 2006, pp. 146–156.

[120] Kumar, M., H. Zhao, and C. Persson. Study of band-structure, optical properties and native defects in $A^IB^{III}O_2$ (A^I = Cu or Ag, B^{III} = Al, Ga or In) delafossites. *Semiconductor Science and Technology*, Vol. 28, No. 6, 2013, id. 065003.

[121] Sheets, W. C., E. Mugnier, A. Barnabé, T. J. Marks, and K. R. Poeppelmeier. Hydrothermal synthesis of delafossite-type oxides. *Chemistry of Materials*, Vol. 18, No. 1, 2005, pp. 7–20.

[122] Read, C. G., Y. Park, and K. S. Choi. Electrochemical synthesis of p-type $CuFeO_2$ electrodes for use in a photoelectrochemical cell. *The Journal of Physical Chemistry Letters*, Vol. 3, No. 14, 2012, pp. 1872–1876.

[123] Gu, J., A. Wuttig, J. W. Krizan, Y. Hu, Z. M. Detweiler, R. J. Cava, et al. Mg-doped $CuFeO_2$ photocathodes for photoelectrochemical reduction of carbon dioxide. *The Journal of Physical Chemistry C*, Vol. 117, No. 24, 2013, pp. 12415–12422.

[124] Prévot, M. S., X. A. Jeanbourquin, W. S. Bourée, F. Abdi, D. Friedrich, R. van de Krol, et al. Evaluating charge carrier transport and surface states in $CuFeO_2$ photocathodes. *Chemistry of Materials*, Vol. 29, No. 11, 2017, pp. 4952–4962.

[125] Omeiri, S., B. Bellal, A. Bouguelia, Y. Bessekhouad, and M. Trari. Electrochemical and photoelectrochemical characterization of $CuFeO_2$ single crystal. *Journal of Solid State Electrochemistry*, Vol. 13, No. 9, 2008, pp. 1395–1401.

[126] Fugate, E. A., S. Biswas, M. C. Clement, M. Kim, D. Kim, A. Asthagiri, et al. The role of phase impurities and lattice defects on the electron dynamics and photochemistry of $CuFeO_2$ solar photocathodes. *Nano Research*, Vol. 12, No. 9, 2019, pp. 2390–2399.

[127] Jiang, C. M., S. E. Reyes-Lillo, Y. Liang, Y. S. Liu, G. Liu, F. M. Toma, et al. Electronic structure and performance bottlenecks of $CuFeO_2$ photocathodes. *Chemistry of Materials*, Vol. 31, No. 7, 2019, pp. 2524–2534.

[128] Hiraga, H., T. Makino, T. Fukumura, H. Weng, and M. Kawasaki. Electronic structure of the delafossite-type $CuMO_2$ (M = Sc, Cr, Mn, Fe, and Co): Optical absorption measurements and first-principles calculations. *Physical Review B*, Vol. 84, No. 4, 2011, id. 041411.

[129] Husek, J., A. Cirri, S. Biswas, A. Asthagiri, and L. R. Baker. Hole thermalization dynamics facilitate ultrafast spatial charge separation in $CuFeO_2$ solar photocathodes. *The Journal of Physical Chemistry C*, Vol. 122, No. 21, 2018, pp. 11300–11304.

[130] Ito, M., C. Izawa, and T. Watanabe. Direct fabrication of a $CuFeO_2$/Fe photocathode for solar hydrogen production by hydrothermal method. *Chemistry Letters*, Vol. 46, No. 6, 2017, pp. 814–816.

[131] Wuttig, A., J. W. Krizan, J. Gu, J. J. Frick, R. J. Cava, and A. B. Bocarsly. The effect of Mg-doping and Cu nonstoichiometry on the photoelectrochemical response of $CuFeO_2$. *Journal of Materials Chemistry A*, Vol. 5, No. 1, 2017, pp. 165–171.

[132] Prévot, M. S., N. Guijarro, and K. Sivula. Enhancing the performance of a robust sol-gel-processed p-type delafossite $CuFeO_2$ photocathode for solar water reduction. *ChemSusChem*, Vol. 8, No. 8, 2015, pp. 1359–1367.

[133] Deng, Z., X. Fang, S. Wu, Y. Zhao, W. Dong, J. Shao, et al. Structure and optoelectronic properties of Mg-doped $CuFeO_2$ thin films prepared by sol–gel method. *Journal of Alloys and Compounds*, Vol. 577, 2013, pp. 658–662.

[134] Mohamed, H., E. Chikoidze, A. Ratep, A. Elsoud, M. Boshta, and M. Osman. Synthesis of conducting single-phase $CuFeO_2$ thin films by spray pyrolysis technique. *Materials Science in Semiconductor Processing*, Vol. 107, 2020, id. 104831.

[135] Barnabé, A., E. Mugnier, L. Presmanes, and P. Tailhades. Preparation of delafossite $CuFeO_2$ thin films by RF-sputtering

on conventional glass substrate. *Materials Letters*, Vol. 60, No. 29–30, 2006, pp. 3468–3470.
[136] Hermans, Y., A. Klein, H. P. Sarker, M. N. Huda, H. Junge, T. Toupance, et al. Pinning of the fermi level in $CuFeO_2$ by polaron formation limiting the photovoltage for photochemical water splitting. *Advanced Functional Materials*, Vol. 30, No. 10, 2020, id. 1910432.
[137] Benko, F. and F. Koffyberg. Opto-electronic properties of p- and n-type delafossite, $CuFeO_2$. *Journal of Physics and Chemistry of Solids*, Vol. 48, No. 5, 1987, pp. 431–434.
[138] Jiang, T., Y. Zhao, M. Liu, Y. Chen, Z. Xia, and H. Xue. Enhancing the lifetime of photoinduced charge carriers in $CuFeO_2$ nanoplates by hydrothermal doping of Mg for photoelectrochemical water reduction. *Physica Status Solidi (a)*, Vol. 215, No. 14, 2018, id. 1800056.
[139] Jang, Y. J., Y. B. Park, H. E. Kim, Y. H. Choi, S. H. Choi, and J. S. Lee. Oxygen-intercalated $CuFeO_2$ photocathode fabricated by hybrid microwave annealing for efficient solar hydrogen production. *Chemistry of Materials*, Vol. 28, No. 17, 2016, pp. 6054–6061.
[140] Rudradawong, C. and C. Ruttanapun. Effect of excess oxygen for $CuFeO_{2.06}$ delafossite on thermoelectric and optical properties. *Physica B: Condensed Matter*, Vol. 526, 2017, pp. 21–27.
[141] Cheng, X., J. Ding, Y. Wu, H. Liu, and G. Dawson. The photocathodic properties of a Fe_2O_3 wrapped $CuFeO_2$ layer on ITO glass for water splitting. *Chemical Physics*, Vol. 513, 2018, pp. 241–245.
[142] Aqaei, F., M. Zare, and A. Shafiekhani. Role of plasmonic Au nanoparticles embedded in the diamond-like carbon overlayer in the performance of $CuFeO_2$ solar photocathodes. *Journal of Solid State Electrochemistry*, Vol. 25, No. 4, 2021, pp. 1139–1150.
[143] Oh, Y., W. Yang, J. Tan, H. Lee, J. Park, and J. Moon. Boosting visible light harvesting in p-type ternary oxides for solar-to-hydrogen conversion using inverse opal structure. *Advanced Functional Materials*, Vol. 29, No. 17, 2019, id. 1900194.
[144] Oh, Y., W. Yang, J. Kim, S. Jeong, and J. Moon. Enhanced photocurrent of transparent $CuFeO_2$ photocathodes by self-light-harvesting architecture. *ACS Applied Materials & Interfaces*, Vol. 9, No. 16, 2017, pp. 14078–14087.
[145] Oh, Y., W. Yang, J. Tan, H. Lee, J. Park, and J. Moon. Photoelectrodes based on 2D opals assembled from Cu-delafossite double-shelled microspheres for an enhanced photoelectrochemical response. *Nanoscale*, Vol. 10, No. 8, 2018, pp. 3720–3729.
[146] Prévot, M. S., Y. Li, N. Guijarro, and K. Sivula. Improving charge collection with delafossite photocathodes: a host–guest $CuAlO_2/CuFeO_2$ approach. *Journal of Materials Chemistry A*, Vol. 4, No. 8, 2016, pp. 3018–3026.
[147] Zhang, L., H. Cao, Y. Lu, H. Zhang, G. Hou, Y. Tang, et al. Effective combination of $CuFeO_2$ with high temperature resistant Nb-doped TiO_2 nanotube arrays for CO_2 photoelectric reduction. *Journal of Colloid and Interface Science*, Vol. 568, 2020, pp. 198–206.
[148] Kang, U., S. K. Choi, D. J. Ham, S. M. Ji, W. Choi, D. S. Han, et al. Photosynthesis of formate from CO_2 and water at 1% energy efficiency via copper iron oxide catalysis. *Energy & Environmental Science*, Vol. 8, No. 9, 2015, pp. 2638–2643.
[149] Yang, X., E. A. Fugate, Y. Mueanngern, and L. R. Baker. Photoelectrochemical CO_2 reduction to acetate on iron–copper oxide catalysts. *ACS Catalysis*, Vol. 7, No. 1, 2016, pp. 177–180.
[150] Kang, U. and H. Park. A facile synthesis of $CuFeO_2$ and CuO composite photocatalyst films for the production of liquid formate from CO_2 and water over a month. *Journal of Materials Chemistry A*, Vol. 5, No. 5, 2017, pp. 2123–2131.
[151] Oh, S., H. Kang, W. Joo, and Y. Joo. Photoelectrochemical CO_2 reduction via $Cu_2O/CuFeO_2$ hierarchical nanorods photocatalyst. *ChemCatChem*, Vol. 12, No. 20, 2020, pp. 5185–5191.
[152] Yoon, S. H., U. Kang, H. Park, A. Abdel-Wahab, and D. S. Han. Computational density functional theory study on the selective conversion of CO_2 to formate on homogeneously and heterogeneously mixed $CuFeO_2$ and CuO surfaces. *Catalysis Today*, Vol. 335, 2019, pp. 345–353.
[153] Baiano, C., E. Schiavo, C. Gerbaldi, F. Bella, G. Meligrana, G. Talarico, et al. Role of surface defects in CO_2 adsorption and activation on $CuFeO_2$ delafossite oxide. *Molecular Catalysis*, Vol. 496, 2020, id. 111181.
[154] Chang, X., T. Wang, and J. Gong. CO_2 photo-reduction: Insights into CO_2 activation and reaction on surfaces of photocatalysts. *Energy & Environmental Science*, Vol. 9, No. 7, 2016, pp. 2177–2196.
[155] Bernstein, N. J., S. A. Akhade, and M. K. Janik. Density functional theory study of carbon dioxide electrochemical reduction on the Fe(100) surface. *Physical Chemistry Chemical Physics*, Vol. 16, No. 27, 2014, pp. 13708–13717.
[156] Berglund, S. P., F. F. Abdi, P. Bogdanoff, A. Chemseddine, D. Friedrich, and R. van de Krol. Comprehensive evaluation of $CuBi_2O_4$ as a photocathode material for photoelectrochemical water splitting. *Chemistry of Materials*, Vol. 28, No. 12, 2016, pp. 4231–4242.
[157] Cooper, J. K., Z. Zhang, S. Roychoudhury, C. M. Jiang, S. Gul, Y.S. Liu, et al. $CuBi_2O_4$: electronic structure, optical properties, and photoelectrochemical performance limitations of the photocathode. *Chemistry of Materials*, Vol. 33, No. 3, 2021, pp. 934–945.
[158] Jung, H. J., Y. Lim, B. U. Choi, H. B. Bae, W. Jung, S. Ryu, et al. Direct identification of antisite cation intermixing and correlation with electronic conduction in $CuBi_2O_4$ for photocathodes. *ACS Applied Materials & Interfaces*, Vol. 12, No. 39, 2020, pp. 43720–43727.
[159] Arai, T., Y. Konishi, Y. Iwasaki, H. Sugihara, and K. Sayama. High-throughput screening using porous photoelectrode for the development of visible-light-responsive semiconductors. *Journal of Combinatorial Chemistry*, Vol. 9, No. 4, 2007, pp. 574–581.
[160] Oropeza, F. E., N. Y. Dzade, A. Pons-Martí, Z. Yang, K. H. L. Zhang, N. H. de Leeuw, et al. Electronic structure and interface energetics of $CuBi_2O_4$ photoelectrodes. *The Journal of Physical Chemistry C*, Vol. 124, No. 41, 2020, pp. 22416–22425.
[161] Sharma, G., Z. Zhao, P. Sarker, B. A. Nail, J. Wang, M. N. Huda, et al. Electronic structure, photovoltage, and photocatalytic hydrogen evolution with p-$CuBi_2O_4$ nanocrystals. *Journal of Materials Chemistry A*, Vol. 4, No. 8, 2016, pp. 2936–2942.

[162] Cao, D., N. Nasori, Z. Wang, Y. Mi, L. Wen, Y. Yang, et al. p-type $CuBi_2O_4$: an easily accessible photocathodic material for high-efficiency water splitting. *Journal of Materials Chemistry A*, Vol. 4, No. 23, 2016, pp. 8995–9001.

[163] Hossain, M. K., G. F. Samu, K. Gandha, S. Santhanagopalan, J. P. Liu, C. Janáky, et al. Solution combustion synthesis, characterization, and photocatalytic activity of $CuBi_2O_4$ and its nanocomposites with CuO and α-Bi_2O_3. *The Journal of Physical Chemistry C*, Vol. 121, No. 15, 2017, pp. 8252–8261.

[164] Wang, F., W. Septina, A. Chemseddine, F. F. Abdi, D. Friedrich, P. Bogdanoff, et al. Gradient self-doped $CuBi_2O_4$ with highly improved charge separation efficiency. *Journal of The American Chemical Society*, Vol. 139, No. 42, 2017, pp. 15094–15103.

[165] Rodríguez-Gutiérrez, I., R. García-Rodríguez, M. Rodríguez-Pérez, A. Vega-Poot, G. Rodríguez Gattorno, B. A. Parkinson, et al. Charge transfer and recombination dynamics at inkjet-printed $CuBi_2O_4$ electrodes for photoelectrochemical water splitting. *The Journal of Physical Chemistry C*, Vol. 122, No. 48, 2018, pp. 27169–27179.

[166] Wang, Y., H. Wang, A. R. Woldu, X. Zhang, and T. He. Optimization of charge behavior in nanoporous $CuBi_2O_4$ photocathode for photoelectrochemical reduction of CO_2. *Catalysis Today*, Vol. 335, 2019, pp. 388–394.

[167] Xu, Y., J. Jian, F. Li, W. Liu, L. Jia, and H Wang. Porous $CuBi_2O_4$ photocathodes with rationally engineered morphology and composition towards high-efficiency photoelectrochemical performance. *Journal of Materials Chemistry A*, Vol. 7, No. 38, 2019, pp. 21997–22004.

[168] Zhang, Z., S. A. Lindley, R. Dhall, K. Bustillo, W. Han, E. Xie, et al. Beneficial CuO phase segregation in the ternary p-type oxide photocathode $CuBi_2O_4$. *ACS Applied Energy Materials*, Vol. 2, No. 6, 2019, pp. 4111–4117.

[169] Hahn, N. T., V. C. Holmberg, B. A. Korgel, and C. B. Mullins. Electrochemical synthesis and characterization of p-$CuBi_2O_4$ thin film photocathodes. *The Journal of Physical Chemistry C*, Vol. 116, No. 10, 2012, pp. 6459–6466.

[170] Park, H. S., C. Y. Lee, and E. Reisner. Photoelectrochemical reduction of aqueous protons with a CuO|$CuBi_2O_4$ heterojunction under visible light irradiation. *Physical Chemistry Chemical Physics*, Vol. 16, No. 41, 2014, pp. 22462–22465.

[171] Li, J., M. Griep, Y. Choi, and D. Chu. Photoelectrochemical overall water splitting with textured $CuBi_2O_4$ as a photocathode. *Chemical Communications*, Vol. 54, No. 27, 2018, pp. 3331–3334.

[172] Kang, D., J. C. Hill, Y. Park, and K. S. Choi. Photoelectrochemical properties and photostabilities of high surface area $CuBi_2O_4$ and Ag-doped $CuBi_2O_4$ photocathodes. *Chemistry of Materials*, Vol. 28, No. 12, 2016, pp. 4331–4340.

[173] Wang, F., A. Chemseddine, F. F. Abdi, R. van de Krol, and S. P. Berglund. Spray pyrolysis of $CuBi_2O_4$ photocathodes: improved solution chemistry for highly homogeneous thin films. *Journal of Materials Chemistry A*, Vol. 5, No. 25, 2017, pp. 12838–12847.

[174] Gottesman, R., I. Levine, M. Schleuning, R. Irani, D. Abou-Ras, T. Dittrich, et al. Overcoming phase-purity challenges in complex metal oxide photoelectrodes: a case study of $CuBi_2O_4$. *Advanced Energy Materials*, Vol. 11, No. 11, 2021, id. 2003474.

[175] Zhang, Z., S. A. Lindley, D. Guevarra, K. Kan, A. Shinde, J. M. Gregoire, et al. Fermi level engineering of passivation and electron transport materials for p-type $CuBi_2O_4$ employing a high-throughput methodology. *Advanced Functional Materials*, Vol. 30, No. 24, 2020, id. 2000948.

[176] Lamers, M., M. Sahre, M. J. Müller, D. Abou-Ras, R. van de Krol, and F. F. Abdi. Influence of post-deposition annealing on the photoelectrochemical performance of $CuBi_2O_4$ thin films. *APL Materials*, Vol. 8, No. 6, 2020, id. 061101.

[177] Lee, J., H. Yoon, K. S. Choi, S. Kim, S. Seo, J. Song, et al. Template engineering of $CuBi_2O_4$ single-crystal thin film photocathodes. *Small*, Vol. 16, No. 39, 2020, id. 2002429.

[178] Gottesman, R., A. Song, I. Levine, M. Krause, A. T. M. N. Islam, D. Abou-Ras, et al. Pure $CuBi_2O_4$ photoelectrodes with increased stability by rapid thermal processing of Bi_2O_3/CuO grown by pulsed laser deposition. *Advanced Functional Materials*, Vol. 30, No. 21, 2020, id. 1910832.

[179] Zhang, Q., B. Zhai, Z. Lin, X. Zhao, and P. Diao. Dendritic $CuBi_2O_4$ array photocathode coated with conformal TiO_2 protection layer for efficient and stable photoelectrochemical hydrogen evolution reaction. *The Journal of Physical Chemistry C*, Vol. 125, No. 3, 2021, pp. 1890–1901.

[180] Song, A., P. Plate, A. Chemseddine, F. Wang, F. F. Abdi, M. Wollgarten, et al. Cu:NiO as a hole-selective back contact to improve the photoelectrochemical performance of $CuBi_2O_4$ thin film photocathodes. *Journal of Materials Chemistry A*, Vol. 7, No. 15, 2019, pp. 9183–9194.

[181] Song, A., I. Levine, R. van de Krol, T. Dittrich, and S. P. Berglund. Revealing the relationship between photoelectrochemical performance and interface hole trapping in $CuBi_2O_4$ heterojunction photoelectrodes. *Chemical Science*, Vol. 11, No. 41, 2020, pp. 11195–11204.

[182] Oropeza, F. E., B. T. Feleki, K. H. L. Zhang, E. J. M. Hensen, and J. P. Hofmann. Influence of reduced Cu surface states on the photoelectrochemical properties of $CuBi_2O_4$. *ACS Applied Energy Materials*, Vol. 2, No. 9, 2019, pp. 6866–6874.

[183] Feng, K., E. M. Akinoglu, F. Bozheyev, L. Guo, M. Jin, X. Wang, et al. Magnetron sputtered copper bismuth oxide photocathodes for solar water reduction. *Journal of Physics D: Applied Physics*, Vol. 53, No. 49, 2020, id. 495501.

[184] Zhang, Q., B. Zhai, Z. Lin, X. Zhao, and P. Diao. CuO/$CuBi_2O_4$ bilayered heterojunction as an efficient photocathode for photoelectrochemical hydrogen evolution reaction. *International Journal of Hydrogen Energy*, Vol. 46, No. 21, 2021, pp. 11607–11620.

[185] Monny, S. A., L. Zhang, Z. Wang, B. Luo, M. Konarova, A. Du, et al. Fabricating highly efficient heterostructured $CuBi_2O_4$ photocathodes for unbiased water splitting. *Journal of Materials Chemistry A*, Vol. 8, No. 5, 2020, pp. 2498–2504.

[186] Malashchonak, I., E. Streltsov, A. Mazanik, O. Korolik, A. Kulak, D. Puzikova, et al. Effective p-type photocurrent sensitization of n-Bi_2O_3 with p-$CuBi_2O_4$ and p-CuO: Z-scheme photoelectrochemical system. *Journal of Solid State Electrochemistry*, Vol. 24, No. 2, 2020, pp. 401–409.

[187] Yang, F., X. Yu, Z. Liu, J. Niu, T. Zhang, J. Nie, et al. Preparation of Z-scheme $CuBi_2O_4$/Bi_2O_3 nanocomposites using electrospinning and their enhanced photocatalytic performance. *Materials Today Communications*, Vol. 26, 2021, id. 101735.

[188] Nishikawa, M., S. Yuto, T. Hasegawa, W. Shiroishi, H. Honghao, Y. Nakabayashi, et al. Compositing effects of

$CuBi_2O_4$ on visible-light responsive photocatalysts. *Materials Science in Semiconductor Processing*, Vol. 57, 2017, pp. 12–17.

[189] Lai, Y. H., K. C. Lin, C. Y. Yen, and B. J. Jiang. A tandem photoelectrochemical water splitting cell consisting of $CuBi_2O_4$ and $BiVO_4$ synthesized from a single $Bi_4O_5I_2$ nanosheet template. *Faraday Discussions*, Vol. 215, 2019, pp. 297–312.

[190] Lee, W. H., J. Kang, H. S. Park, K. M. Nam, and S. K. Cho. Photoelectrochemical response of Au-decorated $CuBi_2O_4$ photocathode in bicarbonate solution. *Journal of Electroanalytical Chemistry*, Vol. 838, 2019, pp. 172–177.

[191] Wang, Y., H. Wang, and T. He. Study on nanoporous $CuBi_2O_4$ photocathode coated with TiO_2 overlayer for photoelectrochemical CO_2 reduction. *Chemosphere*, Vol. 264, 2021, id. 128508.

[192] Díaz-García, A. K., T. Lana-Villarreal, and R. Gómez. Sol-gel copper chromium delafossite thin films as stable oxide photocathodes for water splitting. *Journal of Materials Chemistry A*, Vol. 3, No. 39, 2015, pp. 19683–19687.

[193] Varga, A., G. F. Samu, and C. Janáky. Rapid synthesis of interconnected $CuCrO_2$ nanostructures: a promising electrode material for photoelectrochemical fuel generation. *Electrochimica Acta*, Vol. 272, 2018, pp. 22–32.

[194] Lekse, J. W., M. K. Underwood, J. P. Lewis, and C. Matranga. Synthesis, characterization, electronic structure, and photocatalytic behavior of $CuGaO_2$ and $CuGa_{1-x}Fe_xO_2$ (x = 0.05, 0.10, 0.15, 0.20) delafossites. *The Journal of Physical Chemistry C*, Vol. 116, No. 2, 2012, pp. 1865–1872.

[195] Bredar, A. R. C., M. D. Blanchet, R. B. Comes, and B. H. Farnum. Evidence and influence of copper vacancies in p-type $CuGaO_2$ mesoporous films. *ACS Applied Energy Materials*, Vol. 2, No. 1, 2018, pp. 19–28.

[196] Kumagai, H., G. Sahara, K. Maeda, M. Higashi, R. Abe, and O. Ishitani. Hybrid photocathode consisting of a $CuGaO_2$ p-type semiconductor and a Ru(II)–Re(I) supramolecular photocatalyst: non-biased visible-light-driven CO_2 reduction with water oxidation. *Chemical Science*, Vol. 8, No. 6, 2017, pp. 4242–4249.

[197] Rezaul Karim, K. M., H. R. Ong, H. Abdullah, A. Yousuf, C. K. Cheng, and M. Rahman Khan. Photoelectrochemical reduction of carbon dioxide to methanol on p-type $CuFe_2O_4$ under visible light irradiation. *International Journal of Hydrogen Energy*, Vol. 43, No. 39, 2018, pp. 18185–18193.

[198] Tarek, M., K. M. Rezaul Karim, S. M. Sarkar, A. Deb, H. R. Ong, H. Abdullah, et al. Hetero-structure CdS–$CuFe_2O_4$ as an efficient visible light active photocatalyst for photoelectrochemical reduction of CO_2 to methanol. *International Journal of Hydrogen Energy*, Vol. 44, No. 48, 2019, pp. 26271–26284.

[199] Rezaul Karim, K. M., M. Tarek, H. R. Ong, H. Abdullah, A. Yousuf, C. K. Cheng, et al. Photoelectrocatalytic reduction of carbon dioxide to methanol using $CuFe_2O_4$ modified with graphene oxide under visible light irradiation. *Industrial & Engineering Chemistry Research*, Vol. 58, No. 2, 2018, pp. 563–572.

[200] Karim, K. M., M. Tarek, S. Sarkar, R. Mouras, H. R. Ong, H. Abdullah, et al. Photoelectrocatalytic reduction of CO_2 to methanol over $CuFe_2O_4$@PANI photocathode. *International Journal of Hydrogen Energy*. Vol. 46, No. 48, 2021, pp. 24709–24720.

[201] Thanh Truc, N. T., N. T. Hanh, M. V. Nguyen, N. T. P. le Chi, N. van Noi, D.T. Tran, et al. Novel direct Z-scheme $Cu_2V_2O_7$/g-C_3N_4 for visible light photocatalytic conversion of CO_2 into valuable fuels. *Applied Surface Science*, Vol. 457, 2018, pp. 968–974.

[202] Kormányos, A., A. Thomas, M. N. Huda, P. Sarker, J. P. Liu, N. Poudyal, et al. Solution combustion synthesis, characterization, and photoelectrochemistry of $CuNb_2O_6$ and $ZnNb_2O_6$ nanoparticles. *The Journal of Physical Chemistry C*, Vol. 120, No. 29, 2016, pp. 16024–16034.

[203] Kamimura, S., N. Murakami, T. Tsubota, and T. Ohno. Fabrication and characterization of a p-type $Cu_3Nb_2O_8$ photocathode toward photoelectrochemical reduction of carbon dioxide. *Applied Catalysis B: Environmental*, Vol. 174–175, 2015, pp. 471–476.

[204] Park, J. E., Y. Hu, J. W. Krizan, Q. D. Gibson, U. T. Tayvah, A. Selloni, et al. Stable hydrogen evolution from an $AgRhO_2$ photocathode under visible light. *Chemistry of Materials*, Vol. 30, No. 8, 2018, pp. 2574–2582.

[205] Cheng, X., H. Shen, W. Dong, F. Zheng, L. Fang, X. Su, et al. Nano-Au and ferroelectric polarization mediated Si/ITO/$BiFeO_3$ tandem photocathode for efficient H_2 production. *Advanced Materials Interfaces*, Vol. 3, No. 19, 2016, id. 1600485.

[206] Das, S., P. Fourmont, D. Benetti, S. G. Cloutier, R. Nechache, Z. M. Wang, et al. High performance $BiFeO_3$ ferroelectric nanostructured photocathodes. *The Journal of Chemical Physics*, Vol. 153, No. 8, 2020, id. 084705.

[207] Ida, S., K. Yamada, T. Matsunaga, H. Hagiwara, Y. Matsumoto, and T. Ishihara. Preparation of p-type $CaFe_2O_4$ photocathodes for producing hydrogen from water. *Journal of The American Chemical Society*, Vol. 132, No. 49, 2010, pp. 17343–17345.

[208] Sekizawa, K., T. Nonaka, T. Arai, and T. Morikawa. Structural improvement of $CaFe_2O_4$ by metal doping toward enhanced cathodic photocurrent. *ACS Applied materials & interfaces*, Vol. 6, No. 14, 2014, pp. 10969–10973.

[209] Wheeler, G. P. and K-S. Choi. Investigation of p-type $Ca_2Fe_2O_5$ as a photocathode for use in a water splitting photoelectrochemical cell. *ACS Applied Energy Materials*, Vol. 1, No. 9, 2018, pp. 4917–4923.

[210] Yoon, J-S., Y-M. Kim, J-W. Lee, and Y-M. Sung. A novel strategy for enhancing photoelectrochemical performance of $Ca_2Fe_2O_5$ photocathodes: An integrated experimental and DFT-based approach. *Applied Surface Science*, Vol. 589, 2022, id. 153012.

[211] Pawar, G. S. and A. A. Tahir. Unbiased spontaneous solar fuel production using stable $LaFeO_3$ photoelectrode. *Scientific Reports*, Vol. 8, No. 1, 2018, id. 3501.

[212] Pawar, G. S., A. Elikkottil, S. Seetha, K. S. Reddy, B. Pesala, A. A. Tahir, et al. Enhanced photoactivity and hydrogen generation of $LaFeO_3$ photocathode by plasmonic silver nanoparticle incorporation. *ACS Applied Energy Materials*, Vol. 1, No. 7, 2018, pp. 3449–3456.

[213] Wijten, J. H. J., R. P. H. Jong, G. Mul, and B. M. Weckhuysen. Cathodic electro-deposition of Ni-Mo on semiconducting $NiFe_2O_4$ for photo-electrochemical hydrogen evolution in alkaline media. *ChemSusChem*, Vol. 11, No. 8, 2018, pp. 1374–1381.

[214] Wang, L., H. Tang, and Y. Tian. Carbon-shell-decorated p-semiconductor $PbMoO_4$ nanocrystals for efficient and stable

photocathode of photoelectrochemical water reduction. *Journal of Power Sources*, Vol. 319, 2016, pp. 210–218.

[215] Yuan, J., P. Wang, C. Hao, and G. Yu. Photoelectrochemical reduction of carbon dioxide at $CuInS_2$/graphene hybrid thin film electrode. *Electrochimica Acta*, Vol. 193, 2016, pp. 1–6.

[216] Yuan, J. and Y. Wang. Photoelectrochemical reduction of carbon dioxide to methanol at CuS/CuO/$CuInS_2$ thin film photocathodes. *Journal of The Electrochemical Society*, Vol. 164, No. 13, 2017, pp. E475–E479.

[217] An, C., J. Yuan, and J. Zhu. Reduction of CO_2 to ethanol on Cu-In/$CuInS_2$ composite thin film photocathode. *Journal of The Electrochemical Society*, Vol. 165, No. 16, 2018, pp. H1066–H1071.

[218] Yuan, J., C. Gu, W. Ding, and C. Hao. Photo-electrochemical reduction of carbon dioxide into methanol at $CuFeO_2$ nanoparticle-decorated $CuInS_2$ thin-film photocathodes. *Energy & Fuels*, Vol. 34, No. 8, 2020, pp. 9914–9922.

[219] de Brito, J. F., M. A. S. Andrade Jr, M. V. B. Zanoni, and L. H. Mascaro. All-solution processed $CuGaS_2$-based photoelectrodes for CO_2 reduction. *Journal of CO_2 Utilization,* Vol. 57, 2022, id. 101902.

[220] Lai, Y., N. B. Watkins, C. Muzzillo, M. Richter, K. Kan, L. Zhou, et al. Molecular coatings improve the selectivity and durability of CO_2 reduction chalcogenide photocathodes. *ACS Energy Letters*, Vol. 7, No. 3, 2022, pp. 1195–1201.

[221] Hu, Z., J. Gong, Z. Ye, Y. Liu, X. Xiao, and J. C. Yu. Cu(In,Ga)Se_2 for selective and efficient photoelectrochemical conversion of CO_2 into CO. *Journal of Catalysis*, Vol. 348, 2020, pp. 88–95.

[222] Pati, P. B., Q. Rang, E. Boutin, S. Diring, S. Jobic, N. Barreau, et al. Photocathode functionalized with a molecular cobalt catalyst for selective carbon dioxide reduction in water. *Nature Communications*, Vol. 11, No. 1, 2020, pp. 1–9.

[223] Arai, T., S. Tajima, S. Sato, K. Uemura, T. Morikawa, and T. Kajino. Selective CO_2 conversion to formate in water using a CZTS photocathode modified with a ruthenium complex polymer. *Chemical communications*. Vol. 47, No. 47, 2011, pp. 12664–12666.

[224] Zhou, S., K. Sun, J. Hung, X. Lu, B. Xie, D. Zhang, et al. Accelerating electron-transfer and tuning product selectivity through surficial vacancy engineering on CZTS/CdS for photoelectrochemical CO_2 reduction. *Small*, Vol. 17, 2021, id. 2100496.

[225] Ikeda, S., S. Fujikawa, T. Harada, T. H. Nguyen, S. Nakanishi, T. Takayama, et al. Photocathode characteristics of a spray-deposited Cu_2ZnGeS_4 thin film for CO_2 reduction in a CO_2-saturated aqueous solution. *ACS Applied Energy Materials*, Vol. 2, No. 9, 2019, pp. 6911–6918.

[226] Chen, Y., X. Feng, M. Liu, J. Su, and S. Shen. Towards efficient solar-to-hydrogen conversion: fundamentals and recent progress in copper-based chalcogenide photocathodes. *Nanophotonics*, Vol. 5, No. 4, 2016, pp. 524–547.

[227] Galante, M. T., P. V. Santiago, V. Y. Yukuhiro, L. A. Silva, N. A. Dos Reis, C. T. Pires, et al. Aminopolysiloxane as Cu_2O photocathode overlayer: photocorrosion inhibitor and low overpotential CO_2-to-formate selectivity promoter. *ChemCatChem*, Vol. 13, No. 3, 2021, pp. 859–863.

[228] Pan, H. and C. J. Barile. Electrochemical CO_2 reduction on polycrystalline copper by modulating proton transfer with fluoropolymer composites. *ACS Applied Energy Materials*, Vol. 5, No. 4, 2022, pp. S1–S10.

[229] Kecsenovity, E., B. Endrődi, P. S. Tóth, Y. Zou, R. AW. Dryfe, K. Rajeshwar, et al. Enhanced photoelectrochemical performance of cuprous oxide/graphene nanohybrids. *Journal of The American Chemical Society*, Vol. 139, No. 19, 2017, pp. 6682–6692.

[230] Raciti, D. and C. Wang. Recent advances in CO_2 reduction electrocatalysis on copper. *ACS Energy Letters*, Vol. 3, No. 7, 2018, pp. 1545–1556.

[231] Cheng, D., Z-J. Zhao, G. Zhang, P. Yang, L. Li, H. Gao, et al. The nature of active sites for carbon dioxide electroreduction over oxide-derived copper catalysts. *Nature Communications*, Vol. 12, No. 1, 2021, pp. 1–8.

[232] Sequeda, I. N., and A. M. Meléndez. Understanding the role of copper vacancies in photoelectrochemical CO_2 reduction on cuprous oxide. *The Journal of Physical Chemistry Letters*, Vol. 13, 2022, pp. 3667–3673.